

RESEARCH ARTICLE

10.1002/2016JB013322

Key Points:

- Theoretical models are developed for time-dependent swelling due to adsorption coupling stress-strain-chemical potential-diffusion
- Experiments confirm that the swelling rates are controlled by diffusion of unadsorbed molecules in nanopores
- The diffusion coefficient obtained using our model is independent of gas pressure and adsorbed concentration

Correspondence to:

J. Liu,
j.liu1@uu.nl

Citation:

Liu, J., P. A. Fokker, and C. J. Spiers (2017), Coupling of swelling, internal stress evolution, and diffusion in coal matrix material during exposure to methane, *J. Geophys. Res. Solid Earth*, 122, 844–865, doi:10.1002/2016JB013322.

Received 30 JUN 2016

Accepted 11 JAN 2017

Accepted article online 13 JAN 2017

Published online 3 FEB 2017

Coupling of swelling, internal stress evolution, and diffusion in coal matrix material during exposure to methane

Jinfeng Liu¹ , Peter A. Fokker^{1,2}, and Christopher J. Spiers¹
¹Department of Earth Sciences, Faculty of Geosciences, Utrecht University, Utrecht, Netherlands, ²Netherlands Institute of Applied Geosciences, TNO—National Geological Survey, Utrecht, Netherlands

Abstract We construct theoretical models for time-dependent swelling of coal matrix material upon adsorption of a single gas, taking into account a coupling between stress, strain, chemical potential, and diffusion. Two models are developed. The first (model A) corresponds to diffusion and hence swelling rates being controlled by the jump frequency of adsorbed molecules between closely spaced adsorption sites and the second (model B) to transport controlled by diffusion of unadsorbed molecules through diffusion paths linking distant adsorption sites. To test these models, we performed axial swelling experiments on a single 4 mm sized cylindrical sample of medium volatile bituminous coal, exposed to CH₄ at pressures up to 40 MPa, at 40°C, using 1-D, high-pressure dilatometry. The models were calibrated to the experimental data by adjustment of a single-valued diffusion coefficient, independent of gas pressure and adsorbed concentration. The results show that the data can be accurately explained only by model B. The implication is that the gas transport, the associated adsorption, and hence time-dependent swelling are controlled by the diffusion of unadsorbed molecules and not by molecules jumping between the adjacent adsorption sites. Our model describes a full coupling between stress, strain, sorption, and diffusion in coal matrix material in terms of parameters that have clear physical meaning and are easily obtained from sorption and swelling experiments on coal of any rank exposed to any gas. It therefore offers an important tool for modeling permeability evolution with time during (enhanced) coalbed methane operations.

1. Introduction

It is well established that the adsorption of gases, such as CH₄, CO₂, N₂, and H₂O, by coal can cause swelling strains of up to 1–5% and that this swelling develops in a time-dependent manner reflecting the time dependence of the adsorption process [Day *et al.*, 2010; Fry *et al.*, 2009; Hol and Spiers, 2012; van Bergen *et al.*, 2009]. The kinetics of coal matrix swelling and shrinkage due to gas adsorption and desorption can strongly influence the evolution of coal seam permeability during coalbed methane (CBM) production and CO₂-enhanced CBM production [e.g., Espinoza *et al.*, 2014; Liu *et al.*, 2011; Peng *et al.*, 2014]. Understanding the swelling kinetics of coal matrix material, in a quantitative way, is therefore of central importance for modeling reservoir behavior during both CBM and enhanced CBM (ECBM) operations.

Time-dependent sorption and the associated swelling by coal are generally considered to be controlled by diffusion, as experimental studies show that sorption and swelling rates strongly depend on coal sample or particle size [Busch and Gensterblum, 2011; Busch *et al.*, 2004; Gruskiewicz *et al.*, 2009; Liu *et al.*, 2016a]. Since transport through open fractures or cleats in coal is relatively rapid, the key parameter describing the diffusion kinetics is the diffusion coefficient for the intervening coal matrix. Many experimental studies have been performed on the sorption kinetics of coal with respect to CH₄, CO₂, and N₂ [cf. Busch and Gensterblum, 2011]. These typically focus on the evolution of sorbed concentration, i.e., the approach to equilibrium, that follows a step change in gas pressure applied to an unconfined granular coal sample. The (apparent) diffusion coefficient controlling sorption rate by the coal grains is then calculated by fitting a diffusion model to the transient sorption data. The most widely applied diffusion models are the so-called unipore and bidisperse models [cf. Busch and Gensterblum, 2011]. The first assumes that diffusion in the coal matrix occurs through a network of unimodally distributed nanometer-scale pores, whereas the second assumes a bimodal distribution of macroscale (~30–50 nm) versus microscale (~1–30 nm) pore sizes supporting different diffusion mechanisms and rates (specifically fast diffusion through the macropores controlled by molecule-molecule collision or viscous flow, accompanied by slow diffusion through the micropores).

controlled by molecule/pore-wall collisions or surface diffusion [cf. *Clarkson and Bustin, 1999; Cui et al., 2004; Shi and Durucan, 2003*]). Both the unipore and bidisperse modeling approaches are based on Fick's laws of diffusion within the pore networks considered [cf. *Busch and Gensterblum, 2011*]. Both assume (a) that the driving force for diffusion is the concentration gradient of the diffusing (gas) species within the coal and (b) that any effects of sorption-induced swelling of the coal matrix and associated internal stress development are negligible [e.g., *Busch and Gensterblum, 2011; Busch et al., 2004; Clarkson and Bustin, 1999; Cui et al., 2004; Shi and Durucan, 2003*]. Both analytical and numerical methods have been used to explore the behavior predicted by these models and to calculate the relevant (apparent) diffusion coefficients by fitting to experimental data [*Clarkson and Bustin, 1999*]. The (apparent) diffusion coefficients obtained are generally found to depend not only on coal rank, gas species, and temperature but also on applied gas pressure/density and adsorbed concentration [e.g., *Busch and Gensterblum, 2011; Busch et al., 2004; Clarkson and Bustin, 1999; Cui et al., 2004; Shi and Durucan, 2003; Staib et al., 2013*]. The observed dependence on gas pressure is generally argued to be caused by (a) changes in diffusion mechanism in the coal due to changes in the mean free path of diffusing gas molecules upon changes in external gas pressure [*Clarkson and Bustin, 1999; Cui et al., 2004*] and/or (b) dilation and constriction of transport paths caused by shrinkage and swelling of the coal due to gas desorption and adsorption [*Busch et al., 2004; Shi and Durucan, 2003*]. However, none of the models described above consider the potential effects of swelling and internal stress evolution within the coal on sorption capacity or on the driving force for the diffusion process.

In addition to the above treatments of the kinetics of diffusion-controlled adsorption in coal as a multiscale porous material, coal has also been treated as a polymeric material into which gas can diffuse [e.g., *Goodman et al., 2006; Karacan, 2003; Larsen et al., 1985; Mazumder et al., 2011*]. In polymers, a transition from a glassy phase to a rubbery phase occurs when solvent molecules penetrate the polymer structure, causing polymer swelling [*Haward and Young, 2012*]. This swelling effect leads to diffusion of the dissolved species not obeying Fick's equations, as the driving force for diffusion in this case is provided by the gradient in both solute concentration and swelling stress [*Govindjee and Simo, 1993; Hui et al., 1987a, 1987b; Thomas and Windle, 1982*]. This glass-rubber phase transition behavior of polymers has been applied to interpret coal swelling due to CO₂ adsorption, by assuming that coal matrix material behaves as a glassy polymer that undergoes this transition when CO₂ diffuses or dissolves into it [*Goodman et al., 2006; Karacan, 2007; Larsen, 2004; Mazumder et al., 2011*]. *Mazumder et al. [2011]* applied the above non-Fickian diffusion model for polymers to describe CO₂ diffusion in coal, taking into account the effect of swelling stress on diffusion. However, it still remains unclear whether or not the phase transition assumed to occur in coal due to sorption of CO₂ or other gases (such as CH₄ and N₂) actually does occur [*Hol et al., 2012a*]. Furthermore, *Mazumder et al. [2011]* do not present experiments and have no calibration of their model.

In line with the above-mentioned effect of swelling stress on sorption and diffusion in polymers, recent research has independently demonstrated that the sorption capacity of coal matrix material, with respect to CH₄ and CO₂, is influenced by stresses supported by the solid framework [*Hol et al., 2011, 2012b; Liu et al., 2016b; Pone et al., 2009*]. This effect of applied stress on adsorbed concentration at equilibrium has been explained in terms of thermodynamic theory by *Hol et al. [2012b]* and *Liu et al. [2016b]*. These authors showed that applied compressive stress increases the adsorption energy of adsorbed molecules and hence reduces adsorbed concentration at thermodynamic equilibrium. The magnitude of this effect was shown to depend on the swelling strain contributed by per molecule adsorbed. This means that local sorption-induced swelling within a coal particle or sample can potentially influence diffusion in the coal, because internal swelling stresses generated by nonuniform swelling can change the local chemical potential and equilibrium concentration of the adsorbed molecules, and hence the driving force for their diffusion.

Compared to studies on sorption kinetics, far fewer studies have been conducted on the kinetics of coal matrix swelling due to adsorption. Recently, *Staib et al. [2014]* investigated the effects of gas pressure and coal rank on the swelling kinetics of coal by performing swelling tests on centimeter-scale samples ($3 \times 1 \times 1$ cm³) at gas pressures up to 15 MPa at 55°C, using an optical cell. They qualitatively compared swelling rates at different gas pressures by plotting normalized swelling (i.e., instantaneous volumetric strain per gas pressure step, normalized with respect to the strain achieved at equilibrium) versus time. As observed in studies of adsorption kinetics, *Staib et al. [2014]* also found that swelling rates depended on gas pressure. However, no models currently exist relating the external swelling response to the inwardly progressing

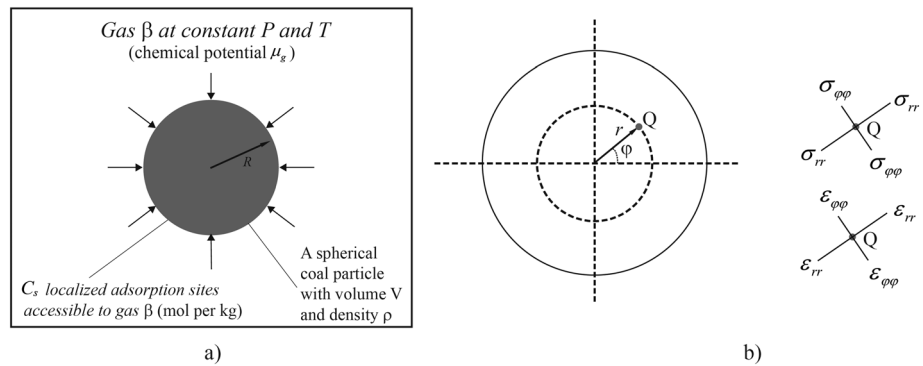


Figure 1. Spherical coal matrix sample/particle geometry used in the present analysis of time-dependent swelling of a particle upon diffusion-controlled penetration and adsorption of a single-gas species β . (a) The assumed spherically symmetric particle or sample geometry. (b) Spherical coordinate and stress/strain reference frame, illustrated in 2-D section. Note that the spherical symmetry implies that the stress and strain components normal to the plane of the diagram are tangential components $\sigma_{\phi\phi} = \sigma_{\gamma\gamma}$ and $\epsilon_{\phi\phi} = \epsilon_{\gamma\gamma}$.

diffusion flux and associated inwardly progressing, adsorption, swelling, and internal stress evolution. In other words, no models are available for predicting the time-dependent swelling behavior of coal matrix material upon exposure to a single gas, or for quantitatively interpreting experimental data such as that reported by *Staib et al.* [2014], despite the fact that swelling behavior plays such an important role in coal seam permeability evolution during (E)CBM production.

In the present study, we investigate the coupling between coal matrix swelling, internal stress evolution, adsorption, and diffusion. We first construct theoretical models for the time-dependent swelling of a coal matrix particle exposed to a single adsorbing gas, allowing for these effects. Two models are developed, covering two basic mechanisms for diffusive transport of gas molecules inside the coal matrix. To determine which mechanism controls the diffusion process, swelling experiments were performed on a single, 4 mm by 4 mm cylindrical sample of medium volatile bituminous coal, from Pingdingshan, China. This was exposed to CH_4 gas at pressures cycled up and down in the range of 0 to 40 MPa, and at a constant temperature of 40°C, using 1-D, high-pressure eddy-current dilatometry to measure the swelling response. The results obtained are compared with our model predictions. This suggests that time-dependent swelling of coal matrix material due to adsorption of a single gas is controlled not by the jump frequency of adsorbed gas molecules between adsorption sites but by the diffusion of unadsorbed gas molecules, with this being characterized by a pressure-independent diffusion coefficient.

2. Theoretical Models

We start by developing theoretical models for time-dependent swelling of a coal matrix particle exposed to a pure gas/fluid phase. We take into account not only diffusion and adsorption but also the coupling between stress, strain, and sorption capacity embodied in the thermodynamic theory by *Hol et al.* [2012b] and *Liu et al.* [2016b]. Two models are derived based on two possible mechanisms for diffusion occurring inside the coal matrix material. We formulate our models for an isotropic, spherically symmetric coal particle or sample geometry, as it is clear and simple from both physical and mathematical standpoints. For simplicity, we henceforth use the term “gas” to cover both gas and (supercritical) fluid.

2.1. Starting Assumptions

We consider the spherical coal particle geometry specified in Figure 1. The particle consists of a small coal matrix sphere (e.g., 0.5–5 mm) of volume V (m^3) and bulk density ρ (kg/m^3), surrounded by a pure gas phase (β) at constant pressure P , absolute temperature T , and chemical potential μ_g . The density of the coal particle is assumed constant during the sorption processes despite small volumetric changes caused by adsorption-induced swelling. The matrix material is considered homogeneous in structure and composition at the particle length scale and isotropic in diffusion and mechanical properties, the latter being linear elastic. It is further assumed to contain nanopores (pore size <30 nm) only, so that there is no Darcian flow and

negligible storage of free, unadsorbed gas. In other words, the coal particle is so small that it is cleat free and can take up gas only by diffusion and adsorption. Lastly, we assume that the coal hosts C_s localized adsorption sites (mol) per kilogram; each of which consists of a potential well capable of trapping a single molecule of the gas β via sorption. C_s is assumed to depend solely on coal rank and gas species. Note that we treat the adsorbed gas molecule as being a “dissolved” component of the solid phase here, following the rigorous thermodynamic treatment by Myers [2002] of stress-free sorption, as opposed to assuming an independently identifiable adsorbed phase. Focusing now on an infinitesimally small representative volume of coal within the spherical particle, located at the generic point Q in Figure 1, for example, then the corresponding pointwise potential of adsorbed molecules is given by Liu et al. [2016b], in J/mol, as

$$\mu_s = \mu_s^{P_0} + (\bar{\sigma} - P_0)V_0 + RT \ln \left(\frac{\theta}{1 - \theta} \right) \quad (1)$$

Here the quantity θ represents the pointwise adsorption site occupancy, R is the gas constant, and the term $RT \ln \left(\frac{\theta}{1 - \theta} \right)$ is the molar configurational entropy of the adsorbed molecules. The quantity V_0 (m^3/mol) represents the partial molar volume of adsorbed gas molecules, which, as in the chemistry of solutions, is identified as the volumetric swelling of the matrix per mole of molecules taken up. The term $(\bar{\sigma} - P_0)V_0$ accordingly represents the stress-strain work done on the surroundings as coal swells against the total local mean stress $\bar{\sigma}$, i.e., $\bar{\sigma} = \frac{\sigma_{rr} + 2\sigma_{\phi\phi}}{3}$. The quantity $\mu_s^{P_0}$ represents the potential of adsorbed molecules at reference pressure $P_0 = 0.1$ MPa, which depends solely on temperature for a given gas. From equation (1), it is clear that the pointwise chemical potential of the adsorbed species (μ_s) depends not only on site occupancy, as in classical sorption models that neglect solid stresses in excess of the applied gas pressure [Myers, 2002], but also on the total mean stress $\bar{\sigma}$. The magnitude of this stress effect further depends on the partial molar volume of the adsorbed molecules V_0 , i.e., the swelling caused by adsorption of 1 mole of gas.

Assuming that V_0 is insensitive to both stress state and adsorbed occupancy [Hol and Spiers, 2012; Liu et al., 2016b; Hol et al., 2012b] and that the volumetric swelling of a small (pointwise) volume dV of coal upon adsorption of n moles of the sorbing species is fully defined as nV_0 , then the pointwise volumetric strain $d\epsilon_v^{\text{ads}}$ can be written as $C_s \rho V_0 \theta$ [Hol and Spiers, 2012; Hol et al., 2012b]. For a millimeter-scale spherical particle of coal matrix into which molecules of species β are diffusing radially, the total volumetric strain of the particle due to adsorption as a function of time is accordingly given as

$$\epsilon_v^{\text{ads}}(t) = \frac{1}{V} C_s \rho V_0 \iiint \theta(r, t) dV \quad (2)$$

This means that to obtain complete expressions for time-dependent swelling of a spherical coal particle during adsorption, we need to calculate the adsorbed occupancy $\theta(r, t)$.

2.2. Assumed Diffusion Mechanisms and Governing Equations

We assume two possible elementary transport mechanisms for the diffusing gas species β , consistent with the concept of site adsorption and with previous site-to-site diffusion models [Balluffi et al., 2005; Shewmon, 1989].

2.2.1. Type A Diffusion: Jump-Controlled Diffusion

In this case, we assume that the adsorption sites for species β inside the coal matrix are sufficiently closely spaced and that the rate of diffusion is controlled by the jump frequency of adsorbed molecules out of their adsorption sites into an adjacent sorption site (see Figure 2). Each adsorption site is either empty or is occupied by one adsorbed molecule. The successful jump rate of an adsorbed molecule into an empty adjacent site, and hence the mobility of the adsorbed molecules, is therefore proportional to the concentration $(1 - \theta)$ of empty (unoccupied) adsorption sites. The energy or activation barrier to diffusion here is the depth of the potential well associated with the adsorption sites, and the driving force for diffusion is the difference in chemical potential between adsorbed molecules in adjacent sites, hence the gradient in chemical potential (Figure 2b).

In line with the above and with standard site-to-site diffusion theory [Balluffi et al., 2005; Shewmon, 1989], the inward (radial) diffusion flux of adsorbed molecules \mathbf{J} ($\text{mol m}^{-2} \text{s}^{-1}$), at any point in a coal matrix sample (here a spherical particle), can be expressed as

$$\mathbf{J} = -D(1 - \theta)C_s \rho \frac{\theta}{RT} \nabla \mu_s \quad (3)$$

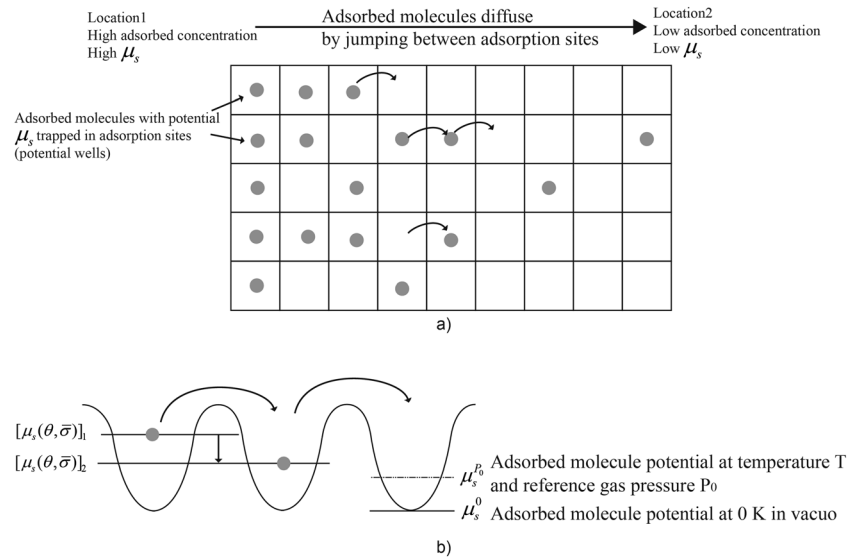


Figure 2. Schematic illustration of type A diffusion. (a) The adsorption sites are so closely spaced that (b) adsorbed molecules diffuse at a rate controlled by the jump process between (out of) adsorption sites. The successful jump rate of adsorbed molecules is proportional to the probability of an adjacent site being empty and is hence to proportional to $(1 - \theta)$, where θ is the site occupancy.

Here the quantity D represents the diffusion coefficient ($\text{m}^2 \text{s}^{-1}$) for random walk, which solely depends on the molecular structure of the coal matrix material, while the term $(1 - \theta)$ represents the jump probability weighting for adsorbed molecules due to the site occupancy effect described above. The term $\frac{D(1-\theta)C_{sp}\theta}{RT}$ represents the phenomenological mobility coefficient relating \mathbf{J} to $\nabla\mu_s$. Note here that when $\theta \ll 1$, i.e., for a “dilute solution,” equation (3) reduces to Fick’s first law expressed in terms of the chemical potential gradient of the diffusing species, i.e., to

$$\mathbf{J} = -DC_{sp} \frac{\theta}{RT} \nabla\mu_s \quad (4)$$

Inserting equation (1) into equation (3), we now obtain

$$\mathbf{J} = -DC_{sp} \left[\frac{\theta(1-\theta)V_0}{RT} \nabla\bar{\sigma} + \nabla\theta \right] \quad (5)$$

which on applying the law of mass conservation for the diffusing species written

$$\frac{\partial\theta}{\partial t} = -\frac{1}{C_{sp}} \nabla \cdot \mathbf{J} \quad (6a)$$

$$\text{yields } \frac{\partial\theta}{\partial t} = -\frac{1}{C_{sp}} \nabla \cdot \mathbf{J} = D \nabla \cdot \left[\frac{\theta(1-\theta)V_0}{RT} \nabla\bar{\sigma} + \nabla\theta \right] \quad (6b)$$

Note here that if sorption induced swelling does not occur, i.e., if the partial molar volume of adsorbed molecules is negligible, so that $V_0 \approx 0$, then the nonlinear term in equations (5) and (6b) disappears. It is also seen from equation (6b) that the pointwise sorption rate $\frac{\partial\theta}{\partial t}$ is influenced not only by diffusion coefficient D but also by adsorption site occupancy θ via the term $\theta(1 - \theta)$.

2.2.2. Type B Diffusion: Path-Controlled Diffusion

In this case, we assume that the adsorption sites are distant from each other and that transport between sorption sites is controlled by diffusion of the unadsorbed molecules through the relatively long intervening diffusion paths (see Figure 3). Here the barrier to diffusion of unadsorbed molecules is the activation barrier for diffusive jumps over the many small barriers (diffusive potential wells) offered by fluctuations in electron field density associated with individual atoms and bonds in the macromolecular coal structure along the diffusion path length. In this case, the driving force for diffusion is the potential gradient of the unadsorbed molecules present in the diffusion path. In any small (pointwise) elementary volume of coal, since jumping of adsorbed molecules out of their sorption sites is assumed to be easy (rapid) compared to longer-range

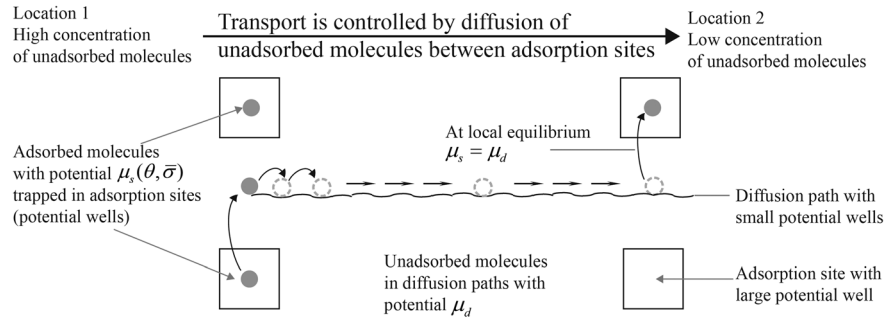


Figure 3. Schematic illustration of type B diffusion. Adsorption sites are distant from each other, so that transport between adsorption sites is controlled by diffusion of unadsorbed molecules along the long, intervening diffusion path. In this case, the potential of unadsorbed molecules must be in local equilibrium with the adsorbed molecules, and the barrier to diffusion is the activation barrier associated with overcoming the many small barriers encountered in the diffusion path.

diffusion of unadsorbed molecules, then the local potential of unadsorbed molecules must equal the potential of the adsorbed molecules (i.e., the adsorbed and unadsorbed species must be in equilibrium). In addition, since there will generally be a far higher concentration of diffusive potential wells in the coal matrix than diffusing molecules, diffusion of unadsorbed molecules is assumed to be treatable as diffusion in a “dilute” solution, with the elementary diffusive steps taken by unadsorbed molecules obeying random walk diffusion (in the absence of a potential gradient).

On the basis of the above, for type B diffusion, the diffusion flux \mathbf{J} ($\text{mol m}^{-2} \text{s}^{-1}$) of unadsorbed molecules can be formulated as

$$\mathbf{J} = -D \frac{C_d}{RT} \nabla \mu_d \quad (7)$$

where C_d (mol m^{-3}) and μ_d (J mol^{-1}) are the pointwise concentration and potential of unadsorbed molecules within the coal. This corresponds to the Fick’s first law expressed in terms of chemical potential. For the present dilute solution of unadsorbed molecules in the diffusion path network, we can further write

$$\mu_d = \mu_{g0} + RT \ln \left(\frac{C_d}{C_{d0}} \right) \quad (8a)$$

$$\text{or } C_d = C_{d0} \exp \left(\frac{\mu_d - \mu_{g0}}{RT} \right) \quad (8b)$$

where μ_{g0} and C_{d0} are the potential and concentration of unadsorbed molecules in the coal at a reference condition corresponding to equilibrium with an external gas phase at reference pressure $P_0 = 0.1 \text{ MPa}$. Inserting equation (8b) into (7), we now obtain

$$\mathbf{J} = -D \frac{C_{d0} \exp \left(\frac{\mu_d - \mu_{g0}}{RT} \right)}{RT} \nabla \mu_d \quad (9)$$

Assuming local equilibrium between the unadsorbed and adsorbed molecules as discussed above, we also have

$$\mu_d = \mu_s \quad (10)$$

which combined with equations (1) and (9) yields

$$\mathbf{J} = -D \frac{C_{d0} \exp \left(\frac{\mu_s - \mu_{g0}}{RT} \right)}{RT} \nabla \mu_s \quad (11a)$$

$$\text{or } \mathbf{J} = -D \frac{C_{d0} \exp \left(\frac{\mu_s^{P_0} + (\bar{\sigma} - P_0)V_0 - \mu_{g0}}{RT} \right)}{RT} \frac{\theta}{1 - \theta} \nabla \mu_s \quad (11b)$$

Writing the equilibrium constant for sorption as $K^0 = \exp \left(\frac{\mu_{g0} - \mu_s^{P_0}}{RT} \right)$, following Liu et al. [2016b], now gives

$$\mu_{g0} - \mu_s^{P_0} = RT \ln K^0 \quad (12)$$

which, inserted equation (11b) and combined with equation (1), leads to the result

$$\mathbf{J} = \frac{-C_{d0}D}{K^0} \exp\left(\frac{(\bar{\sigma} - P_0)V_0}{RT}\right) \left[\frac{\theta V_0}{(1-\theta)RT} \nabla \bar{\sigma} + \frac{1}{(1-\theta)^2} \nabla \theta \right] \quad (13)$$

Finally, assuming that the storage of unadsorbed molecules in the coal matrix is negligible, the conservation of mass requires that the rate of change of adsorbed molecule concentration, at any point, must equal the divergence of diffusion flux, yielding

$$\frac{\partial \theta}{\partial t} = -\frac{1}{C_s \rho} \nabla \cdot \mathbf{J} = \frac{DC_{d0}}{K^0 C_s \rho} \nabla \cdot \left\{ \exp\left(\frac{(\bar{\sigma} - P_0)V_0}{RT}\right) \left[\frac{\theta V_0}{(1-\theta)RT} \nabla \bar{\sigma} + \frac{1}{(1-\theta)^2} \nabla \theta \right] \right\} \quad (14)$$

Note that this equation is highly nonlinear, even if the partial molar volume of adsorbed molecules, and hence the magnitude of sorption-induced swelling, is negligible (i.e., $V_0 \approx 0$). Moreover, the sorption rate $\frac{\partial \theta}{\partial t}$ is influenced not only by the diffusion coefficient D but also by the adsorbed occupancy θ via the terms $\frac{\theta}{(1-\theta)}$ and $\frac{1}{(1-\theta)^2}$. The type B diffusion model thus predicts an increasing diffusion-controlled adsorption rate with increasing sorbed concentration θ .

2.3. Time-Dependent Swelling of a Spherically Symmetric Coal Particle

We now consider how a spherical particle or sample of isotropic coal, as represented in Figure 1, will swell with time when exposed at its outer surface to a gas at constant pressure P . The application of this gas pressure to the outer boundary of the particle will of course drive diffusion of gas molecules radially into the coal particle. The associated sorption will cause a radially symmetric swelling and hence stress-strain field to develop, which will continuously evolve until a uniform equilibrium-sorbed concentration and a uniform swelling strain are achieved throughout the particle. The evolution of the system with time will accordingly be determined by the diffusion equations (equations (6b) and (14)), by the stress-strain behavior of the coal (which we assume to be elastic), and by the initial and boundary conditions imposed on the system, with the externally measured sample volume strain being given by equation (2), for example.

For the case of spherical symmetry, the stress state at any radial coordinate is given by the principal stresses σ_{rr} and $\sigma_{\phi\phi} = \sigma_{\gamma\gamma}$. Displacements u are only possible in the radial direction, and the principal strains are related to radial displacement via $\epsilon_{rr} = \frac{\partial u}{\partial r}$ and $\epsilon_{\phi\phi} = \epsilon_{\gamma\gamma} = \frac{u}{r}$ (note that we take compression as positive and radial displacement to be positive inward). By analogy with the thermo-elastic equations for an isotropic sphere, subjected to an instantaneously imposed fixed temperature at its external surface [e.g., *Hetnarski et al.*, 2009], the following relations for the displacement and total stress fields inside the sample may be obtained (see details of derivation in Appendix A):

$$u(r, t) = -\frac{\alpha}{r^2} \frac{1+\nu}{1-\nu} \int_0^r r^2 \theta(r, t) dr - 2 \frac{\alpha r}{b^3} \frac{1-2\nu}{1-\nu} \int_0^b r^2 \theta(r, t) dr + r(1-2\nu) \frac{P}{E} \quad (15a)$$

$$\sigma_{rr}(r, t) = \frac{-\alpha E}{1-\nu} \left\{ \frac{2}{b^3} \int_0^b r^2 \theta(r, t) dr - \frac{2}{r^3} \int_0^r r^2 \theta(r, t) dr \right\} + P \quad (15b)$$

$$\sigma_{\phi\phi}(r, t) = \frac{-\alpha E}{1-\nu} \left\{ \frac{1}{r^3} \int_0^r r^2 \theta(r, t) dr + \frac{2}{b^3} \int_0^b r^2 \theta(r, t) dr - \theta(r, t) \right\} + P \quad (15c)$$

$$\bar{\sigma} = \frac{-2E\alpha}{1-\nu} \left(\frac{1}{b^3} \int_0^b r^2 \theta dr - \frac{1}{3} \theta \right) + P \quad (15d)$$

$$\tau_{\max} = \frac{1}{2} |\sigma_{rr}(r, t) - \sigma_{\phi\phi}(r, t)| = \frac{\alpha E}{2(1-\nu)} \left[\frac{3}{r^3} \int_0^r r^2 \theta(r, t) dr - \theta(r, t) \right] \quad (15e)$$

where $\alpha = \frac{1}{3} C_s V_0 \rho$, E is the Young's modulus, and ν is the Poisson's ratio.

At the boundary, i.e., at $r = b$, we therefore have

$$u(b, t) = -\frac{3\alpha}{b^2} \int_0^b r^2 \theta(r, t) dr + b(1-2\nu) \frac{P}{E} \quad (16a)$$

$$\epsilon_r(b, t) = -\frac{3\alpha}{b^3} \int_0^b r^2 \theta(r, t) dr + (1-2\nu) \frac{P}{E} \quad (16b)$$

$$\sigma_{rr}(b, t) = P \quad (16c)$$

$$\sigma_{\phi\phi}(b, t) = \frac{-\alpha E}{1 - \nu} \left\{ \frac{3}{b^3} \int_0^b r^2 \theta(r, t) dr - \theta(r, t) \right\} + P \quad (16d)$$

If we now insert the local stress state (equation (15d)) into diffusion equations (6b) and (14), corresponding to type A and B diffusion, respectively, the following relations emerge: For type A diffusion (jump-controlled diffusion): Model A

$$\frac{\partial \theta}{\partial t} = \frac{D}{r^2} \frac{\partial}{\partial r} \left\{ r^2 \left[\left(\frac{2}{9} \frac{EV_0^2 C_s \rho}{1 - \nu} \frac{\theta(1 - \theta)}{RT} + 1 \right) \frac{\partial \theta}{\partial r} \right] \right\} \quad (17a)$$

If the partial molar volume of adsorbed molecules is negligible, i.e., $V_0 \approx 0$, this reduces to

$$\frac{\partial \theta}{\partial t} = \frac{D}{r^2} \frac{\partial}{\partial r} \left(r^2 \frac{\partial \theta}{\partial r} \right) \quad (17b)$$

For type B diffusion (path-controlled diffusion): Model B

$$\frac{\partial \theta}{\partial t} = \frac{DC_{d_0}}{C_s \rho K^0} \frac{1}{r^2} \frac{\partial}{\partial r} \left\{ r^2 \left[\exp \left(\frac{\left(\frac{-2C_s V_0 \rho E}{3(1-\nu)} \left\{ \frac{1}{b^3} \int_0^b r^2 \theta dr - \frac{\theta}{3} \right\} + P - P_0 \right) V_0}{RT} \right) \left(\frac{2}{9} \frac{EV_0^2 C_s \rho}{1 - \nu} \frac{\theta}{(1 - \theta)RT} + \frac{1}{(1 - \theta)^2} \right) \frac{\partial \theta}{\partial r} \right] \right\} \quad (18a)$$

For simplicity, this can be reduced to

$$\frac{\partial \theta}{\partial t} = \frac{DC_{d_0}}{C_s \rho K^0} \frac{1}{r^2} \frac{\partial}{\partial r} \left\{ r^2 \left[\exp \left(\frac{(P - P_0) V_0}{RT} \right) \left(\frac{2}{9} \frac{EV_0^2 C_s \rho}{1 - \nu} \frac{\theta}{(1 - \theta)RT} + \frac{1}{(1 - \theta)^2} \right) \frac{\partial \theta}{\partial r} \right] \right\} \quad (18b)$$

as the term $\left(\frac{1}{b^3} \int_0^b r^2 \theta dr - \frac{\theta}{3} \right)$ is a second-order correction term in case θ is not homogeneous in space and vanishes quickly after a change in external pressure. In addition, if the partial molar volume of the adsorbed molecules is very small (i.e., $V_0 \approx 0$), equation (18b) reduces to

$$\frac{\partial \theta}{\partial t} = \frac{DC_{d_0}}{C_s \rho K^0} \frac{1}{r^2} \frac{\partial}{\partial r} \left[r^2 \left(\frac{1}{(1 - \theta)^2} \frac{\partial \theta}{\partial r} \right) \right] \quad (18c)$$

Note that in both of the above models (equations (17a) and (18b)), the magnitude of the effect of swelling and internal stress evolution on diffusion depends on the term $\frac{2EV_0^2 C_s \rho}{1 - \nu}$. Particle swelling as a function of time and imposed external gas pressure is of course given by equations (16a) and (16b), with $\theta(r, t)$ being given by integrating equations (17a) and (18b).

3. Swelling Experiments on Coal Exposed to CH₄

To test the applicability of the above models, we performed axial swelling experiments on a single cylindrical sample of medium volatile bituminous coal (~4 mm in both diameter and length), exposed to CH₄ at cycled gas pressures up to 40 MPa, and at a constant temperature of 40°C, using 1-D, high-pressure eddy-current dilatometry [Hol and Spiers, 2012]. Note here that we used a 1:1 cylindrical sample because a spherical sample is difficult to make. In these experiments, compressive stresses and gas pressure were measured positive, as were swelling strains.

3.1. Sample Material and Preparation

The coal used in this study was obtained from Pingmei Shenma Mine No. 8 near Pingdingshan City in Henan Province, China. Petrographic and chemical analyses were performed on powdered samples of this material (grain size 170–250 μm), at the China University of Geosciences in Beijing (Table 1). These showed that Pingdingshan coal has a vitrinite reflectance of $1.31 \pm 0.06\%$ and contains 80.32% carbon, 1.52% nitrogen, 0.37% sulfur, and 3.94% oxygen.

To prepare the cylindrical sample, we drilled a core, with a diameter of 4 mm and length of ~6 mm, parallel to bedding and normal to the butt cleat plane, using a water-cooled pillar drill. The ends of the core were ground flat and parallel to produce final dimensions of ~4 mm diameter and ~4 mm length. The sample

Table 1. Organic Petrology, Proximate Analysis, and Ultimate Analysis Performed on a 170–250 μm Grain Size Fraction of the Pingdingshan Medium Volatile Bituminous Coal Used as Sample Material in the Present Study^a

Coal Rank	Medium Volatile Bituminous	
Organic petrology	Vitrinite reflectance Rx %	1.31
	Vitrinite %	90.43
	Moisture %	0.7
Proximate analysis	Volatile matter %, dry	20.65
	Ash content %, dry	12.61
	Fixed carbon %	66.05
Ultimate analysis	Carbon %	80.32
	Nitrogen %	1.52
	Sulfur %	0.37
	Oxygen %	3.94

^aThe analyses were performed at the China University of Geosciences, Beijing.

was then inspected using an optical microscope to exclude the presence of cleats and damage. The cylinder axis was defined as the x direction of the sample. The y direction was defined as lying parallel to the intersection of the bedding and butt cleat planes, while the z direction was taken as normal to bedding (see Figure 4). Prior to experimentation, the sample was dried in an oven at 50°C for several days. The pretest length and diameter of the sample were then measured, using a digital caliper (with a resolution of 0.01 mm), and its mass was measured using a Mettler Toledo MS205DU

Semi-Micro Analytical Balance (resolution 0.01 mg). Averaged values of mass and dimensions obtained from multiple measurements are listed in Table 2. The sample length given in this table was taken as the starting dimension used for all subsequent calculations of strain in the axial (x) direction.

3.2. Experimental Methods

We measured the dimensional change of the sample in the x direction using a high-pressure dilatometer system, described in detail by Hol and Spiers [2012]. This consists of a millimeter-scale sample holder plus a high-pressure eddy-current displacement sensor, housed in a 100 MPa stainless steel pressure vessel. Axial expansion or contraction of the sample, caused by adsorption or desorption of gases introduced into the pressure vessel at high pressure, is transmitted to a Remanit stainless steel target; the motion of which is measured from changes in the eddy-current field induced in the target by the eddy-current sensor. This allows sample expansion and contraction to be measured with a resolution better than 50 nm. The eddy-current sensor yields a linear sensitivity of 19.96 mV/ μm over a displacement range of 120 μm , which is equivalent to an axial strain of $\sim 2.5\%$ for a 4 mm long sample.

In the present experiments, CH_4 was injected into the pressure vessel at pressure up to 40 MPa. Two methods were used to generate the pressure. For pressures up to ~ 9 MPa, CH_4 was introduced into the system directly from a CH_4 cylinder through a manually controlled regulator. This allowed stepwise increases in CH_4 pressure up to ~ 9 MPa (cylinder pressure) with an accuracy of ± 0.01 MPa. To generate higher CH_4 pressures, an ISCO

volumetric (syringe) pump was used in controlled pressure mode, allowing pressure control within ± 0.02 MPa. To maintain a constant temperature in and around the sample of 40°C ($\pm 0.05^\circ\text{C}$), the entire pressure vessel plus internal dilatometer system and sample were placed in a temperature-controlled water bath. The whole setup, including water bath, the ISCO volumetric pump, and the high-pressure tubing system, were housed in a heated foam-polystyrene box, maintained at an internal temperature of $38.6 \pm 0.2^\circ\text{C}$ using a construction lamp and CAL 9900 proportional integral differential temperature controller.

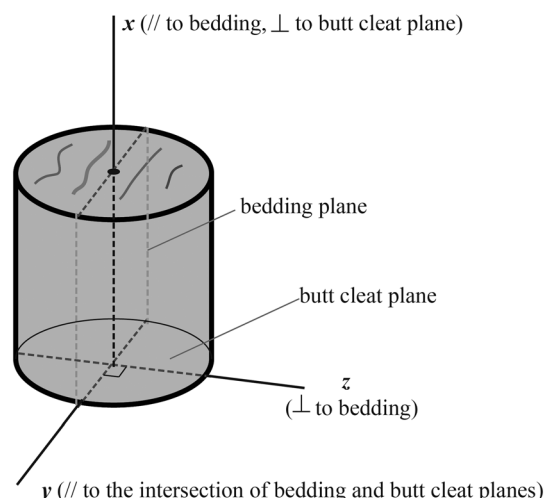


Figure 4. Schematic illustration of the present coal matrix sample geometry.

Table 2. Starting Mass and Dimensions of the Cylindrical Pingdingshan Coal Matrix Sample Used in This Study^a

	Initial Sample Mass (g)	Initial Sample Length L_{0x} (mm)	Initial Sample Diameter $L_{0y} = L_{0z}$ (mm)	Density ρ (kg/m ³)
4–3	0.06792	3.76	4.01	1431.04

^aThe initial length L_0 serves as the starting dimension for all axial swelling strain determinations.

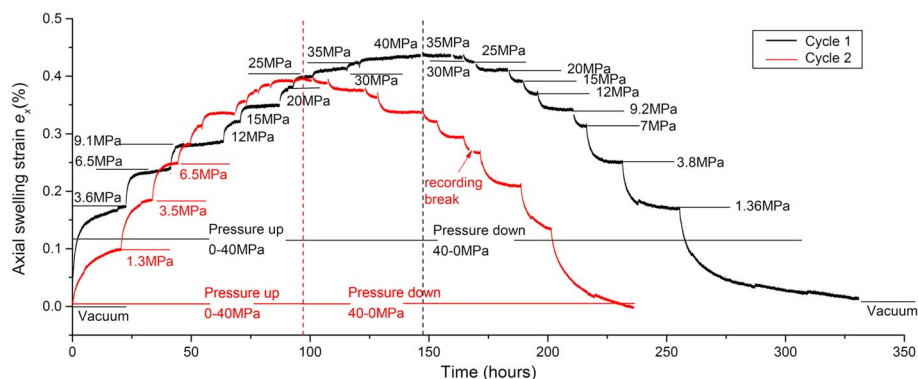
After loading the sample studied into the dilatometer and pressure vessel, the system was evacuated by connecting it to a vacuum pump to remove residual gas and water from the sample and apparatus. This took about 5 h (time to obtain a constant/stable eddy-current sensor signal). CH₄ was then introduced into the system. The CH₄ pressure was then increased stepwise up to 40 MPa. After each pressure step, the sample expanded, in a time-dependent manner, to approach a new equilibrium state. After the equilibration at 40 MPa, the CH₄ pressure was decreased in a stepwise manner, and the vessel/sample finally reevacuated. We assumed that equilibrium was reached or approached when no further change in eddy-current sensor signal was recorded for around 2 h, i.e., when a constant sample strain was reached. We performed two pressurization and depressurization cycles on the single sample investigated, continuously recording the axial dimensional changes of the sample during these pressure cycles. In each cycle, the axial swelling strain (%) of the sample versus time was calculated using the expression $e_x(t) = \frac{V_{t=0} - V(t)}{10 \times S L_{0x}}$, where $V_{t=0}$ represents the output voltage (mV) of the eddy-current sensor at the start of the gas pressure cycle, i.e., in the evacuated state at $t=0$. $V(t)$ represents the sensor output at time t . S represents the sensitivity of the eddy-current sensor, and L_{0x} is the starting axial dimension (length) of the sample specified in Table 2.

3.3. Experimental Results

The axial swelling strain versus time data obtained during the two CH₄ pressure cycles employed in the present experiments are shown in Figure 5. Upon applying each gas pressure step, an instant compaction or expansion was observed, reflecting the elastic response of the sample to the change in hydrostatic pressure. The sample then slowly expanded or contracted. Equilibration after each pressure step took 3–70 h. The swelling strain data attained at (apparent) equilibration are plotted in Figure 6 as a function of CH₄ pressure. During the first pressurization cycle, the (apparent) axial swelling strain continuously increased with increasing pressure, attaining a maximum swelling strain of 0.435% at 40 MPa CH₄ pressure. This swelling was partly irreversible, with the contraction data obtained upon depressurization showing minor hysteresis, as well as 0.014% permanent swelling strain, which corresponds to 3.2% of the maximum swelling strain. By contrast, the swelling that occurred in the second pressure cycle was closely reversible. In this case the maximum swelling strain measured was 0.395% at 40 MPa CH₄ pressure, so ~10% less than the value obtained in the first pressure cycle.

4. Analysis

We now analyze our models and compare our models for swelling of a spherical coal sample with our experimental data for the 4 mm sized coal matrix cylinder subjected to CH₄ pressure cycling. To determine which


Figure 5. Axial swelling strain versus time for the two pressure cycles applied to the coal matrix sample investigated in this study.

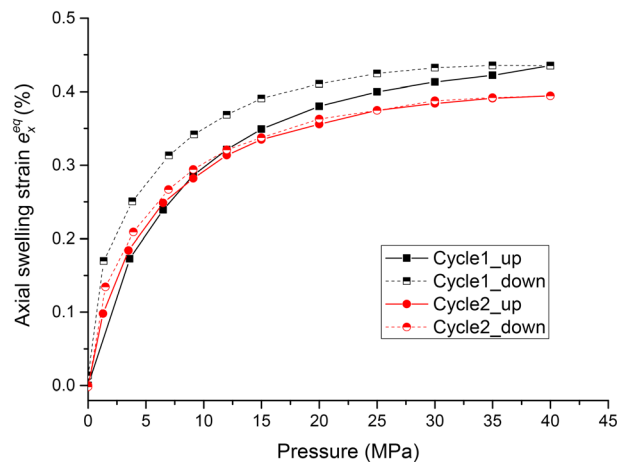


Figure 6. Equilibrium axial swelling strains versus CH₄ pressure for the two pressure cycles applied to the coal matrix cylinder investigated in this study.

spaced and that the rate of diffusion is controlled by the jump frequency of adsorbed molecules out of their adsorption sites into an adjacent sorption site (see Figure 2). Our model B assumes that the adsorption sites are distant from each other and that transport between sorption sites is controlled by diffusion of the unadsorbed molecules through the relatively long intervening diffusion paths (see Figure 3). The differences between two models in diffusion mechanisms suggest that the distribution of adsorption sites plays an important role in the diffusion process of adsorbed molecules inside the coal matrix. If adsorption sites are sufficiently closely spaced, the molecules can be transported between adsorption sites by jumps, and swelling kinetics and diffusion will be described by model A. If the adsorption sites are relatively distant, the adsorbed molecules are transported between adsorption sites by diffusion of unadsorbed molecules in the diffusion paths as the rate controlling step, and the swelling kinetics and diffusion can be described by model B. This implies that the parameter C_s gives an indication regarding the likely mechanism of diffusion, assuming a homogeneous distribution of adsorption sites over the whole coal matrix material. In other words, if the sorption sites are uniformly distributed spatially, then samples in which diffusion is dominated by short range jumping would have a higher C_s than if diffusion is controlled by long-range path diffusion. However, a value of C_s only specifies the total sorption site concentration and does not tell us anything about the distribution of sorption sites.

4.1.2. Role of Swelling and Internal Stress Evolution in Determining the Driving Force for Diffusion

Our models (see equations (15d), (16b), (17a), and (18b)) incorporate the effects of internal stress-strain evolution upon swelling and on the driving force for the diffusion processes. The magnitude of this latter effect on diffusion depends on ratio between the two terms in the right-hand side of equations (17a) and (18b): $\frac{2EV_0^2C_s\rho}{1-\nu} \frac{\theta(1-\theta)}{RT}$. Figure 7a plots $\frac{2EV_0^2C_s\rho}{1-\nu} \frac{\theta(1-\theta)}{RT}$ versus adsorbed occupancy θ at equilibrium for the parameter values used in this study (see Table 3). It is seen from Figure 7a that the effect of swelling on the driving force is small for a value of $V_0 = 11.4 \times 10^{-6} \text{ m}^3/\text{mol}$, with a maximum at $\theta = 0.5$. However, for gas species that have a larger partial molar volume of adsorbed molecules than CH₄ (e.g., >2 times the present V_0 ; see Figure 7b), the swelling effect may play a significant role in diffusion process. In addition, for coal matrix material that has a large E (e.g., $>40 \text{ GPa}$; see Figure 7c), the swelling effect may also play a significant role in diffusion process, even when $V_0 = 11.4 \times 10^{-6} \text{ m}^3/\text{mol}$. However, the effect of swelling on the driving force is small for a value of $E = 12.3 \text{ GPa}$ that we employed in this study (see Figure 7c).

4.1.3. Role of Adsorbed Concentration in Determining Swelling Rates

In addition to the effect of swelling and the internal stress evolution on diffusion described above, model A (jump-controlled diffusion; see equations (16b) and (17b)) demonstrates that particle/sample swelling rates depend on the random walk diffusion coefficient D for adsorbed molecules only, if the effects of swelling and internal stress evolution on diffusion are negligible. In this case, the adsorbed concentration θ plays no role in swelling kinetics. By contrast, model B (path-controlled diffusion; see equations (16b) and (18c)) demonstrates that the swelling rate depends not only on the random walk diffusion coefficient D for

model (type A versus type B diffusion) can describe the experimental data best, the numerical solutions for the diffusion and particle swelling equations presented in section 2.3 (i.e., equations (16b), (17a), and (18b)) must be obtained. This can be achieved by obtaining the best fit between model and experiments, using reasonable parameter values and adjusting D .

4.1. Model A Versus Model B

4.1.1. Role of Distribution of Adsorption Sites

Our model A assumes that the adsorption sites for species β inside the coal matrix are sufficiently closely

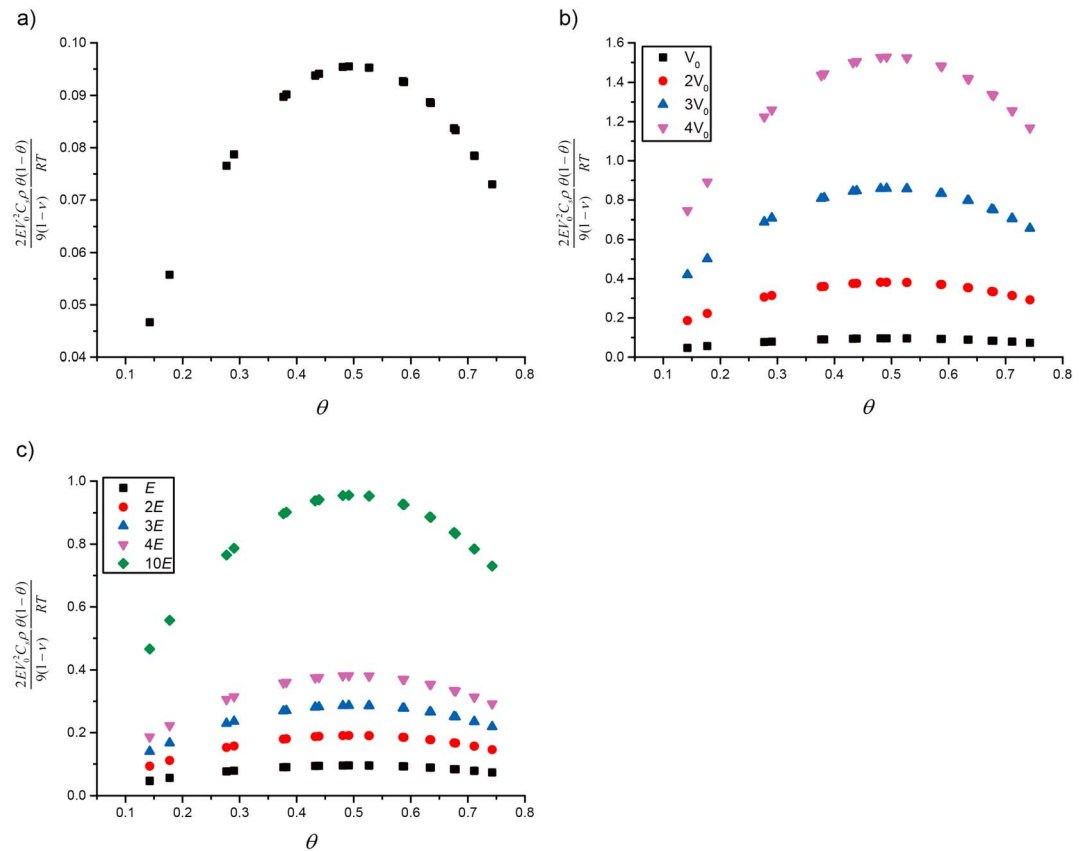


Figure 7. Effects of swelling and internal stress evolution on diffusion. (a) Plot of the quantity $\frac{2E V_0^2 C_0 \rho \theta (1-\theta)}{9(1-\nu) RT}$ versus θ at equilibrium, obtained using the parameter values employed in the present study. (b) Plot of $\frac{2E V_0^2 C_0 \rho \theta (1-\theta)}{9(1-\nu) RT}$ versus θ for varying V_0 . (c) Plot of $\frac{2E V_0^2 C_0 \rho \theta (1-\theta)}{9(1-\nu) RT}$ versus θ for varying E .

unadsorbed molecules but also strongly on the adsorbed concentration θ via the term $1/(1-\theta)^2$. In this case, swelling rates increase with the increasing θ at a given D .

4.2. Comparison With Experiments

The main purpose of this paper is to investigate the coupling between swelling, stress, and diffusion. To achieve this, we developed simple models for the swelling of a spherical particle, focusing on the radially symmetric diffusion problem, as it is clear and simple from both physical and mathematical standpoints (see also section 2). We used a 1:1 cylindrical sample because a spherical sample is difficult to make. At the same time, field equations for diffusion in a cylindrical sample surrounded by gas are difficult to handle because radial symmetry is lost. Of course, our radially symmetric (spherical) diffusion model will not accurately describe 3-D diffusion field in a 1:1 cylindrical sample. However, we believe that the error in modeling radial and axial strain evolution due to diffusion in a cylindrical sample is acceptable. This is underpinned by the fact that model studies on thermal expansion of 4 mm diameter spheres versus 4 mm diameter cylindrical rods, subjected to a stepwise temperature change at the boundary, show a sphere:cylinder strain ratio of ~ 0.8 [cf. Hetnarski *et al.*, 2009]. The usefulness of our approach is also supported by the fact that our simple radially symmetric model explains our experimental data well (see details in section 4.2.2), using a single diffusion coefficient over all boundary conditions.

Table 3. Summary of Parameter Values Applied in the Present Model

Parameter	K^0	C_s (mol/kg _{coal})	E (GPa)	ν	V_0 (m ³ /mol)
Values used in this study	0.01	1.5	12.3	0.233	11.4×10^{-6}

4.2.1. Choice of Fixed Parameter Values

To fit our models to the time-dependent experimental data obtained on swelling strain, we need input parameter values for the elastic constants E , ν , the partial molar volume of the adsorbed molecules V_0 , the adsorbed occupancy at outer boundary $\theta^{\text{eq}}(P)$, the adsorption site density C_s , and the equilibrium constant K^0 . The following paragraphs describe how we obtained values for these parameters (see Table 3).

Hol and Spiers [2012] measured the bulk modulus K_s of bituminous coal matrix cylinders (4 mm in diameter and ~4 mm in length) using helium, obtaining 7.413–7.746 GPa. We took the average value of 7.65 GPa as the bulk modulus of our sample. The uncertainty in the bulk modulus that we employed is small, as the sample used by *Hol and Spiers* [2012] is similar to our sample used in this study, in rank, size, and geometry. *Espinoza et al.* [2014] measured Poisson's ratio ν for bituminous cylindrical coal samples (38 mm in diameter and 76 mm in length), collected from Forzando Mine in South Africa, obtaining 0.267 in radial direction and 0.198 in axial direction. For simplicity, we took the average value of 0.233 as the Poisson's ratio of our sample for the present calculations. This large sample data must represent an underestimate of ν in our smaller matrix sample. However, even increasing ν to 0.3 or 0.4 has little effect on the best fit value of diffusion coefficient D , as seen in equations (17a) and (18b). Using these values of K_s and ν , the Young's modulus E was calculated using $E = 3 K_s(1 - 2\nu)$, yielding $E = 12.3$ GPa.

To obtain values for the parameters C_s , K^0 , and V_0 , independently, we consider the relations for equilibrium-adsorbed concentration or occupancy $\theta^{\text{eq}}(P)$, and for the associated swelling strain $e_{\text{ads}}^{\text{eq}}$, given by *Liu et al.* [2016b] under the present experimental conditions (i.e., $\sigma = P$). These can be written as

$$\theta^{\text{eq}} = \frac{a_g K^0 \exp\left(\frac{-(P-P_0)V_0}{RT}\right)}{1 + a_g K^0 \exp\left(\frac{-(P-P_0)V_0}{RT}\right)} \quad (19a)$$

$$e_{\text{ads}}^{\text{eq}} = V_0 C_s \rho \frac{a_g K^0 \exp\left(\frac{-(P-P_0)V_0}{RT}\right)}{1 + a_g K^0 \exp\left(\frac{-(P-P_0)V_0}{RT}\right)} \quad (19b)$$

where a_g is the activity of CH_4 at pressure P and at 40°C. Now the sorption-induced volumetric swelling strain ($e_{\text{ads}}^{\text{eq}}$) of a cleat-free coal matrix sample can be calculated from the measured swelling strain (e_v) by correcting for the elastic deformation using the expression $e_{\text{ads}}^{\text{eq}} = e_v + P/K_s$ [cf. *Hol and Spiers*, 2012]. Using our experimental data for the swelling strain of our coal matrix sample measured in the x direction (see Figures 6 and 8), and assuming that $e_x = e_y$ and $e_z = 1.2e_x$ [Day et al., 2010], we obtain $e_v = 3.2e_x$ and $e_{\text{ads}}^{\text{eq}} = 3.2e_x + P/K_s$. Since the swelling of our sample was partly irreversible in the first CH_4 pressure cycle but closely reversible in the second pressure cycle (see Figures 5 and 6), we assumed the swelling strains obtained in the second pressure cycle represent (reversible) sorption-induced swelling better, and we applied these data to calculate sorption-induced volumetric swelling strains using the above expression. The estimated adsorption-induced volumetric swelling strains are plotted in Figure 8 as a function of pressure. Taking the thermodynamic reference state defined at $P = 0.1$ MPa, we can also obtain the CH_4 activity (a_g) at the experimentally imposed pressures and at 40°C using the equation of state for CH_4 [Setzmann and Wagner, 1991]. A nonlinear regression method was then used to fit equation (19b) to the estimated data of $e_{\text{ads}}^{\text{eq}}(a_g, P)$ obtained for the second CH_4 pressure cycle. The best fit ($R^2 = 0.998$) gave $C_s = 1.5$ mol/kg_{coal}, $K^0 = 0.01$, and $V_0 = 11.4 \times 10^{-6}$ m³/mol (see Figure 8). These parameter values are consistent with the values reported in the literature: reported ranges are from 0.9 to 2.5 mol/kg_{coal} for C_s , from 0.02 to 0.05 for K^0 , and from 8 to 20×10^{-6} m³/mol for V_0 [Cui et al., 2007; Dutta et al., 2011; Gensterblum et al., 2013; Laxminarayana and Crosdale, 1999; Levine, 1996; Merkel et al., 2015; Pan and Connell, 2007; Pini et al., 2010]. Note that the literature values for C_s and K^0 are obtained from fitting the Langmuir relationship without considering stress effects on sorption and can therefore not be directly compared with our values (see details in *Liu et al.* [2016b]).

4.2.2. Model Results

To obtain solutions for the nonlinear diffusion equations (see equations (17a) and (18b)), we use *pdepe*, a MATLAB function that solves initial-boundary value problems for systems of parabolic and elliptic partial differential equations in one space variable r and time t . The ordinary differential equations resulting from discretization in space are integrated to obtain approximate solutions at specified times. The function returns values of the solution on a predefined mesh. We applied equation (16b) by integrating the *pdepe* output field

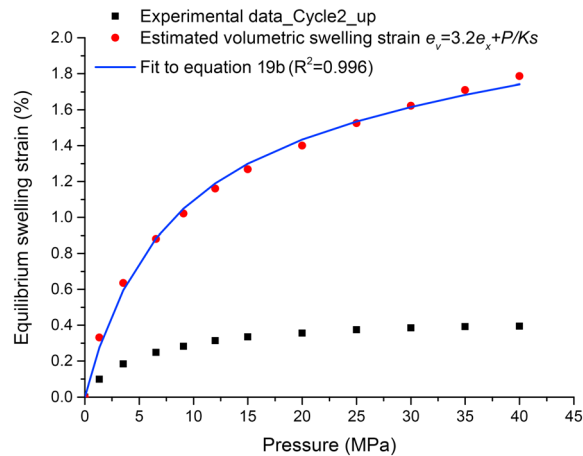


Figure 8. Swelling strain versus CH₄ pressure data for the present cylindrical coal sample, as determined for the second CH₄ pressure cycle. The solid square points represent the swelling strains measured in the x direction in the second CH₄ pressure cycle. The solid red points represent the sorption-induced volumetric swelling strain estimated using $e_{\text{ads}}^{\text{eq}} = 3.2e_x + P/K_s$. The blue line represents the best fit of equation (19b) to the estimated volumetric strain data. The resulting fitting parameter values are summarized in Table 3.

the thermodynamic relation of equation (19a). We fitted our two models to our swelling kinetic data shown in Figure 5 using the least squares method embedded in MATLAB. We used the fixed parameter values listed in Table 3 for all pressure steps. Fits were then created by adjusting the single diffusion coefficient across all pressure steps (i.e., the entire experiments) and resetting the equilibrium occupancy term (θ) corresponding to the change in boundary condition at each pressure step. Model outcomes were calculated at regularly spaced times t_i , spanning the full time range of each experiment (all pressure steps). The measured strain-time data, distributed about each time ordinate t_i , were taken as being recorded at these times. The optimum value of the diffusivity was then determined by minimizing the least squares difference between the model results and the strain measurements associated with each time t_i .

The best fits of the models (A and B) to the experimental data are plotted in Figure 9. The results illustrate that the experimental data are very well explained by model B (path-controlled diffusion) using a single diffusion coefficient over all CH₄ pressures, particularly the data obtained in the second cycle from which the various fixed parameters were calculated. By contrast, model A provides a much poorer fit to the experimental data, which is unsatisfactory. This suggests that swelling of Pingdingshan medium volatile bituminous coal upon adsorption of CH₄ is controlled by diffusion of unadsorbed molecules. The best fit of model B to the experimental data gave a value for $\frac{DC_{d0}}{K^0C_{sp}}$ (effective diffusion coefficient) of $7.17 \times 10^{-12} \text{ m}^2 \text{ s}^{-1}$ for the first CH₄ pressure cycle and of $9.5 \times 10^{-12} \text{ m}^2 \text{ s}^{-1}$ for the second. In this case, we cannot obtain the random walk diffusion coefficient D ($\text{m}^2 \text{ s}^{-1}$) for unadsorbed molecules independently of C_{d0} (mol m^{-3}), as this reference concentration C_{d0} is unknown, although it is a constant.

Finally, note that changing the elastic constants assumed in our spherical diffusion models (see equations (17a) and (18b)) will change the fitted value of D , which is linearly coupled to the elastic constants, but not the quality of the fit. This is visible from the form of equation (17a) versus equation (17b) and equation (18b) versus equation (18c). It is the quality of fit that we used to discriminate between the two models considered.

5. Discussion

We have developed two models for time-dependent swelling of a spherical sample/particle of coal matrix material upon adsorption of a single gas, considering the coupled effects of swelling, internal stress evolution, and diffusion. Model A assumed that the adsorbed molecules were transported inside the coal matrix at a rate controlled by jumps between potential wells associated with closely spaced adsorption sites

over the spatial dimension in order to obtain the sample strain response for comparison with the experimental data. Using equation (16b), and defining the concentration at time t_i and location r_j as $c_{ij} = \alpha \cdot \theta(t_i, r_j)$, we may obtain the simulated radial swelling strain for the spherical particle:

$$\epsilon_{\text{rr}}^{\text{sim}}(t_i) = \frac{1}{V} \sum_j c_{ij} \cdot 4\pi r_j^2 \delta r_j - (1 - 2\nu) \frac{P}{E} \quad (20)$$

In order to solve the diffusion equations, boundary conditions must be applied. We employed an equilibrium occupancy at the boundary, assuming that this level of occupancy is achieved immediately after applying a new external hydrostatic pressure, i.e., $\theta_{r=b} = \theta^{\text{eq}}(P)$. The value of the equilibrium occupancy follows from

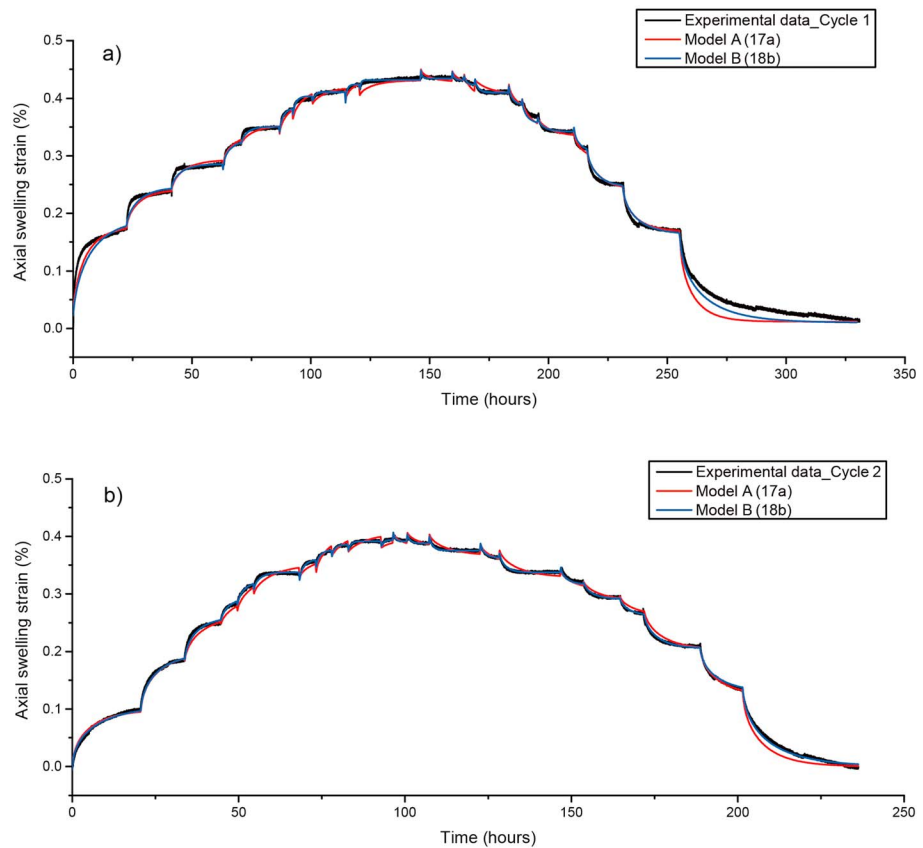


Figure 9. Axial swelling strain (%) versus time (hours) plotted (a) for the first CH_4 pressure cycle and (b) for the second CH_4 pressure cycle. The black lines represent the experimental data. The red lines represent the best fit of model A (equations (17a) and (20)) to the experimental data using a constant D , while the blue lines represent the best fit of model B (equations (18b) and (20)) to the experimental data using a constant D . Note that the fit of model B (path-controlled diffusion) is almost perfect for Cycle 2 from which the fixed (nonfitting) parameters were derived.

(type A diffusion). Model B assumed that the adsorbed molecules were transported at a rate controlled by diffusion of unadsorbed molecules between more distant adsorption sites (type B diffusion). Experimental tests were performed on a single 4 mm sized cylindrical coal matrix cylinder to measure the time-dependent swelling upon adsorption of CH_4 . Comparison of the model results with the experimental data illustrates that model B successfully described time-dependent swelling of Pingdingshan medium volatile bituminous coal upon adsorption of CH_4 at 40°C .

In the following, we will further discuss the mechanisms of diffusion occurring inside the present coal matrix material and the influence of internal stress evolution on transport path. We then attempt to explain the differences in swelling behavior of the coal matrix sample that we measured between the two CH_4 pressure cycles used in our experiments. Finally, we compare our studies with the previous work and we consider the likely implications for ECBM operations.

5.1. Mechanisms for Diffusion Occurring Inside the Coal Matrix Material

Our experimental data are well described by our model B using a single diffusion coefficient over all CH_4 pressure ranges but not by our model A. In addition, the fact that the calculated diffusion product (effective diffusion coefficient) $\frac{DC_{g0}}{K^0 C_{sp}} = 9.5 \times 10^{-12} \text{ m}^2 \text{ s}^{-1}$, obtained using model B, is independent of CH_4 pressure and adsorbed concentration is internally consistent with its assumption that D is the diffusion coefficient for random walk of unadsorbed CH_4 molecules through the coal structure. Furthermore, the better performance of model B suggests that the adsorption sites for CH_4 in the present coal sample are distant from each other or are concentrated into scattered, localized clusters that are distant from each other. This implies that

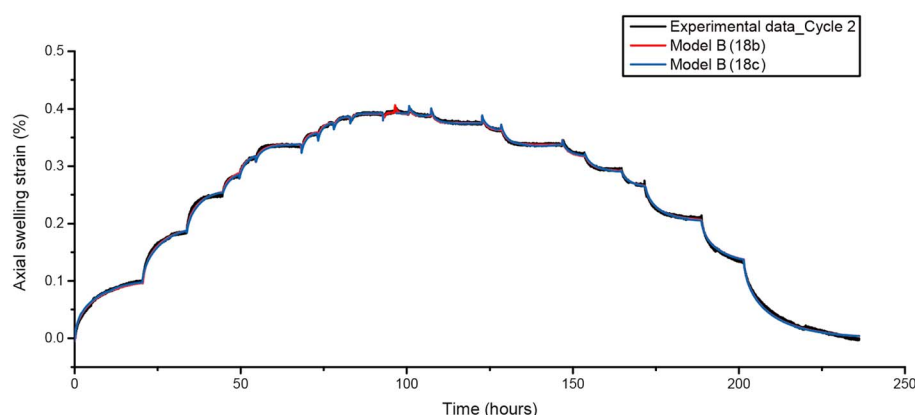


Figure 10. Axial swelling strain versus time comparing fits of equations (18b) and (18c) to the experimental data for the second CH_4 pressure cycle conducted in the present experiments, using the same value for the effective diffusion coefficient. Recall that the second experimental cycle showed closely reversible sorption-induced swelling behavior of the sample and was used to derive the nonfitting parameters used in model B.

adsorbed molecules cannot be transported from adsorption site to adsorption site by direct jumps. In line with the assumptions and equations defining model B, our findings accordingly suggest that (a) the dynamic or transient swelling response of Pingdingshan medium volatile bituminous coal to adsorption of CH_4 is dominated by diffusion of unadsorbed molecules; (b) the driving force for diffusion is the gradient in the potential of unadsorbed molecules, which in the case of path-controlled diffusion is equal to the gradient in the potential of the adsorbed molecules; (c) the driving force is influenced by swelling of the coal matrix and the associated internal stress evolution (see equations (7), (10), and (11a)); (d) the effect of swelling and internal stress evolution on diffusion depends quadratically on the magnitude of the partial molar volume of the adsorbed molecules V_0 (refer to equation (18b)); and (e) net sorption and sorption-induced swelling rates depend on both the diffusion coefficient D and on the adsorbed occupancy θ (equations (16b) and (18b)).

5.2. Effect of Internal Stress Evolution on Changes in Transport Paths

As analyzed in section 4.1.2, the influence of the swelling effect on diffusion is small in the present study, i.e., when $V_0 = 11.4 \times 10^{-6} \text{ mol/m}^3$. This is also supported by the fact, shown in Figure 10, that a similar quality of fits of equation (18b) (model B when $V_0 = 11.4 \times 10^{-6} \text{ mol/m}^3$) versus equation (18c) (model B when $V_0 = 0$) to the experimental data for the second CH_4 pressure cycle use the same value for the effective diffusion coefficient. However, the typical evolution of internal stress field (see Figure 11), as calculated using model B (equations (15b), (15c), (15d), (15e) and (18b)), illustrates large tensile stresses ($>30 \text{ MPa}$) and shear stresses ($>25 \text{ MPa}$). This suggests that tensile microfractures might be formed during diffusion [Zhao *et al.*, 2016]. As a result, the real internal stresses might be lower than the calculated internal stresses. Moreover, the formation of microfractures during first exposure to CH_4 may have caused changes of transport paths for diffusion of unadsorbed molecules as well as permanent deformation of the sample. This would explain the permanent deformation we observed after the first CH_4 pressure cycle and the mismatch of our model B with the swelling data in the first pressure cycle. Reversible deformation upon the real internal stress evolution (i.e., lower than calculated stress) after the formation of microfractures may also be possible [Hol *et al.*, 2012a], explaining (a) the closely reversible swelling of the sample observed during the second CH_4 pressure cycle and (b) the good fit of our model B to the experimental data for Cycle 2.

5.3. Swelling Data for CH_4 Pressure Cycle 1 Versus Cycle 2

Our experimental results showed an irreversible swelling and shrinkage effect during the first CH_4 pressure cycle but not during the second cycle. This irreversible swelling might be caused by the formation of microfractures during the diffusion process [Hol *et al.*, 2012a]. This possibility is supported by the evolution of internal stresses calculated using our model B as discussed in section 5.2.

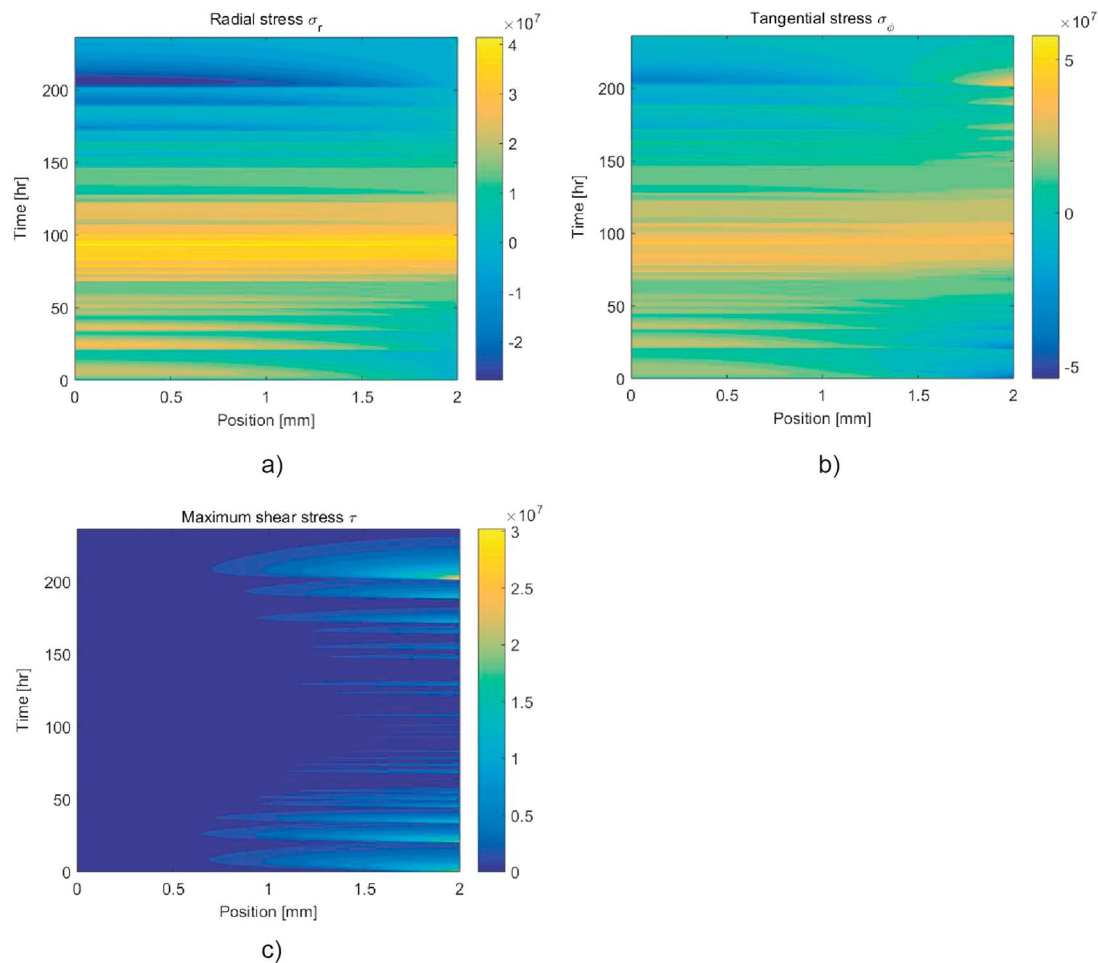


Figure 11. Typical evolution of internal stress field (contour) caused by swelling/shrinkage occurring during diffusion into the spherical coal matrix particle modeled in this study. Recall that compressive stress is positive and tensile stress is negative. (a) Total radial stress calculated using equation (15b). (b) Total tangential stress calculated using equation (15c). (c) Maximum shear stress calculated using equation (15e). Note that x axis represents the position in radial direction, while y axis represents the evolution time, spanning the full time range for each experiment (all pressure steps).

Our experimental results also show that the net linear swelling strains of the sample that we measured during the first cycle were larger than those measured during the second cycle. Recalling that the net linear swelling strains that we measured involved both elastic deformation upon changes in gas pressures and sorption-induced swelling, we propose the following possible causes:

1. Lower equilibrium swelling strains were attained in Cycle 2. This would be in accordance with the fact that the total time elapsed for Cycle 1 was longer than that elapsed for Cycle 2, but the (apparent) diffusion coefficients calculated for both cycles were similar. This might reflect equilibration in Cycle 1 throughout the sample, and so on the full sample length scale, but with CH_4 molecules not penetrating the sample homogeneously. This would also fit with the notion of heterogeneous swelling producing microcrack damage and causing the observed hysteresis and permanent swelling seen in Cycle 1.
2. The elastic modulus of the sample was reduced upon the formation of microfractures during Cycle 1. Indeed, during Cycle 2, clearer and bigger instant elastic responses than in Cycle 1 were observed (Figure 5).
3. Extensional creep occurred during Cycle 1 due to cumulative microcracking. For the first pressure steps of Cycle 1 (6.5 MPa and 9.1 MPa), Figure 5 shows that the sample expanded to an apparent equilibrium swelling strain and then continued to swell with time in a near-linear manner. This behavior might be related to the slow evolution of internal stress state and associated formation of microfractures. If extensional creep by this mechanism would result in permanent swelling, as observed in Cycle 1, it

would not be expected to repeat itself during Cycle 2. However, the observed permanent deformation could also be caused by a residual amount of adsorbed CH₄ remaining in the sample after Cycle 1. This is potentially supported by the small shrinkage observed at the end of Cycle 2 (see Figure 6).

Based on our experiments, we cannot discriminate between these explanations; the only remark we wish to make is that it is probably related to microcracking associated with the large tensile stresses.

5.4. Comparison With Previous Work

The similarities and differences between our findings and previous work can be summarized pointwise as follows:

1. Our model B successfully describe the swelling kinetics of coal matrix material upon adsorption of CH₄ at CH₄ pressures varied in the range of 0 to 40 MPa, using a single, random walk diffusion coefficient describing diffusion of unadsorbed molecules as the rate-limiting process. However, our model B demonstrates that the swelling kinetics also strongly depend on adsorbed concentration. This finding is consistent with reports in the literature that diffusion coefficients calculated using the widely accepted unipore and bidisperse models strongly depend on adsorbed concentration [e.g., *Busch et al.*, 2004; *Clarkson and Bustin*, 1999; *Cui et al.*, 2004; *Shi and Durucan*, 2003].
2. Our models (A and B) consider diffusion occurring inside a single coal matrix particle, containing uniform nanopores only. The agreement obtained between model B and the experimental results suggests that (a) samples of medium bituminous coal matrix material, as used in this study, can be simply treated as containing uniform nanopores only, at least on the ~4 mm length scale and that (b) the swelling kinetics of coal matrix material of medium bituminous rank are dominated by diffusion of unadsorbed molecules in nanopores. This differs from many studies in which diffusion is believed to occur through a bimodal or bidisperse pore network [*Busch et al.*, 2004; *Cui et al.*, 2004; *Shi and Durucan*, 2003]. We cannot eliminate the possibility that other models would also fit our experimental data well, but for our very small matrix samples, which likely contain only micropores/nanopores (<30 nm), our simple, single-mechanism, single fitting parameter diffusion model seems preferable. For bigger coal samples (>4 mm) or for other coals, a bidisperse pore structure model might better represent the heterogeneous properties of coal [*Busch and Gensterblum*, 2011; *Clarkson and Bustin*, 1999; *Cui et al.*, 2004; *Shi and Durucan*, 2003]. In such cases, more complicated mechanisms for diffusion in coal need to be considered, beyond the present study.
3. While our results imply that the swelling kinetics of millimeter-scale coal matrix samples, upon adsorption of CH₄, are controlled by diffusion of unadsorbed molecules through a uniform nanopore network inside the coal matrix, the observed swelling is caused by the absorbed molecules. This may point to the storage of unadsorbed molecules in nanopores being negligible. This would mean that only a few unadsorbed molecules exist in the nanopores, interacting with the molecular structure of the coal and not with each other, and that therefore they do not behave as a gas phase. Under these assumptions, we cannot quantify the diffusion coefficient D using our model B, as the reference concentration of adsorbed molecules C_{d0} is unknown. In the literature, however, coal matrix is generally represented by a bidisperse pore structure model [*Busch and Gensterblum*, 2011; *Clarkson and Bustin*, 1999; *Cui et al.*, 2004; *Shi and Durucan*, 2003]. This model assumes that gas diffuses into the coal matrix in the gas phase. Numerical solutions yield diffusion coefficients for methane in the range of 10^{-12} – 10^{-15} m²/s [cf. *Busch and Gensterblum*, 2011]. Our calculated diffusion product $\frac{DC_{d0}}{K^0C_{s,p}}$ (apparent diffusion coefficient) yields 9.5×10^{-12} m²/s, which is consistent with the previous studies. However, we wish to stress that the real state of unadsorbed molecules diffusing in nanopores and how their state is influenced by pore dimensions remain unknown. To clarify these, an advanced spectroscopy technique or molecular dynamic methods is needed.

5.5. Likely Implications for ECBM

The likely implications of our findings for ECBM are as follows:

1. Our findings suggest that for most coal ranks, the swelling kinetics of coal matrix upon adsorption of CH₄ are dominated by diffusion of unadsorbed molecules. The same is likely true for adsorption of CO₂ and N₂ as the adsorption site density, which may indicate site spacing, falls in the same range of 0.7–3 mol/kg_{coal} for CH₄, CO₂, and N₂ [cf. *Battistutta et al.*, 2010; *Gensterblum et al.*, 2013, 2014]. This suggests that our model B may be widely applied to predict time-dependent swelling of coal matrix upon adsorption of

all of these gases. All parameters in our model B have clear physical meaning and can be easily obtained from swelling or sorption kinetic experiments. This means that our model B offers an important tool for modeling coal seam permeability evolution with time due to the swelling and shrinkage response of coal matrix during ECBM production. However, coal is a naturally heterogeneous material, and the distribution of adsorption sites for gas species cannot be expected to be homogeneous. Some adsorption sites for a gas species might therefore be concentrated into scattered, localized clusters, with internal exchange of adsorbed molecules being controlled by the jump process, while the clusters might be distant, forcing diffusion between clusters to be controlled by diffusion of unadsorbed molecules.

2. Our model B demonstrates that swelling kinetics of coal matrix upon adsorption CH_4 and probably also CO_2 and N_2 depend not only on the diffusion coefficient but also on concentration of the sorbing species, increasing with increasing adsorbed concentration. This suggests that the shrinkage rates of coal matrix upon CBM recovery will decrease with decreasing adsorbed CH_4 concentration, while the swelling rates of coal matrix upon injection of CO_2 will increase with increasing adsorbed concentration of CO_2 . This together with the finding that the diffusion coefficient for CO_2 is generally 1 or 2 orders higher than that for CH_4 [Busch and Gensterblum, 2011] suggests that swelling rates upon CO_2 injection would be much higher than shrinkage rates upon CBM recovery. This, together with the net (equilibrium) swelling effects upon CO_2 injection [Day et al., 2012; Mazumder and Wolf, 2008], in turn implies that using CO_2 for enhanced CBM recovery is unlikely to be a very successful strategy, as indeed reported in previous attempts at CO_2 -ECBM [e.g., Fokker and van der Meer, 2004; Fujioaka et al., 2010; van Bergen et al., 2006]. However, new strategies involving injection of N_2 or N_2 - CO_2 mixtures might enhance both CBM recovery and CO_2 geological storage in coal seam [Day et al., 2012; Liu et al., 2016a; Pini et al., 2011].
3. Our results suggest that for higher-rank coal, the effect of swelling and internal stress evolution upon adsorption and diffusion of CH_4 , CO_2 , and N_2 on driving force for diffusion can be neglected, while for lower-rank coals, this effect might need to be considered. This is because the partial molar volume of adsorbed molecules (i.e., V_0) in low-rank coal is generally higher (by 1–3 times) than that in high-rank coals [cf. Day et al., 2010, 2012; Fry et al., 2009; Hol et al., 2012b; Suuberg et al., 1993] and because the magnitude of the effect of swelling and internal stress development is proportional to V_0^2 (see section 4.1.2.). In both models the swelling rates for low-rank coal might be significantly faster than those for high-rank coal due to the swelling effects on driving force.

6. Conclusions

We investigated the coupling between swelling kinetics, internal stress evolution, and diffusion in coal matrix material during exposure to a single gas by developing theoretical models and performing experimental tests.

Two models were developed, covering two basic possible mechanisms for transport of gas molecules occurring inside the coal matrix. These correspond to transport of adsorbed molecules being controlled by either jumps between adjacent adsorption sites or by diffusion of unadsorbed molecules through longer diffusion paths inside the coal matrix (models A and B, respectively).

Experimental tests were performed on a single cylindrical sample of Chinese Pingdingshan medium volatile bituminous coal. We measured temporal development of axial swelling of the coal matrix (4 mm in diameter and ~4 mm in length) during exposure to CH_4 at a number of CH_4 pressures up to 40 MPa, and at a constant temperature of 40°C, by using high-pressure eddy-current dilatometry. Then, we compared our model predictions with the experimental data. The results show that the observed time-dependent swelling is well explained by model B. This suggests that time-dependent swelling in this case is controlled not by the jumps of adsorbed gas molecules between adsorption sites but by the diffusion of unadsorbed molecules. In addition, our model for diffusion of this type shows that the effect of swelling and associated internal stress evolution on diffusion of CH_4 (and probably of CO_2 and N_2) in the coal such as those used in this study can be neglected, as the partial molar volume of the adsorbed molecules V_0 is small.

Nonetheless, our models demonstrate that (a) the distribution of adsorption sites plays a role in determining the mechanism of diffusion, (b) the effect of swelling and the internal stress evolution contributes to the driving force for diffusion processes independently of the gradient in adsorbed concentration and that the importance of this effect strongly depends on the magnitude of V_0 , and (c) swelling rates of coal matrix material depend not solely on diffusion coefficient but also on adsorbed concentration.

Since all parameters used in our models have well-defined physical meaning and are easily obtained from sorption and swelling experiments, the models can be applied to any coal rank and to any gas. Our models therefore offer an important tool for modeling coal matrix stress-strain evolution and hence coal seam/cleat permeability evolution with time, as influenced by adsorption/desorption and diffusion occurring during CBM and ECBM operations.

Appendix A

For the case of spherical symmetry, the stress state at any radial coordinate is given by the principal stresses σ_{rr} and $\sigma_{\phi\phi} = \sigma_{\gamma\gamma}$. Displacements u are only possible in the radial direction, and the principal strains are related to radial displacement via $\varepsilon_{rr} = \frac{\partial u}{\partial r}$ and $\varepsilon_{\phi\phi} = \varepsilon_{\gamma\gamma} = \frac{u}{r}$ (note that we take compression as positive and radial displacement to be positive inward). Applying Hooke's law for our assumed isotropic, elastically deformable particle now gives

$$\varepsilon_{rr} = \frac{1}{E} (\sigma_{rr} - 2\nu\sigma_{\phi\phi}) - \alpha\theta \quad (\text{A1a})$$

$$\varepsilon_{\phi\phi} = \frac{1}{E} [(1-\nu)\sigma_{\phi\phi} - \nu\sigma_{rr}] - \alpha\theta \quad (\text{A1b})$$

where $\alpha = \frac{1}{3}C_s V_0 \rho$.

Rearranging the above equations and expressing the strains in terms of radial displacements yields the following relations for the radial, tangential, and mean stresses:

$$\sigma_{rr} = \frac{E}{1-2\nu} \left\{ \frac{1-\nu}{1+\nu} \frac{\partial u}{\partial r} + \frac{2\nu}{1+\nu} \frac{u}{r} + \alpha\theta \right\} \quad (\text{A2a})$$

$$\sigma_{\phi\phi} = \frac{E}{1-2\nu} \left\{ \frac{\nu}{1+\nu} \frac{\partial u}{\partial r} + \frac{1}{1+\nu} \frac{u}{r} + \alpha\theta \right\} \quad (\text{A2b})$$

$$\bar{\sigma} = \frac{1}{3} (\sigma_{rr} + 2\sigma_{\phi\phi}) = \frac{E}{1-2\nu} \left\{ \frac{1}{3r^2} \frac{\partial}{\partial r} (r^2 u) + \alpha\theta \right\} \quad (\text{A2c})$$

These equations are exactly equivalent to the thermo-elastic equations for a radially symmetry isotropic body, i.e., a sphere, subjected to an instantaneously imposed fixed temperature at its external surface. In such a system, the thermal gradient leads to the inward conduction of heat and an inward progression of a radially symmetric temperature and stress-strain field, as described by *Hetnarski et al.* [2009], for example. In these authors' treatment, α is the thermal expansion coefficient and θ is the temperature increase.

In addition to equations (A2a)–(A2c), force balance applies everywhere in the interior at the present coal particle, which results in the stress equilibrium equation, $\frac{1}{r^2} \frac{\partial}{\partial r} (r^2 \sigma_{rr}) - \frac{2\sigma_{\phi\phi}}{r} = 0$. Combined with the constitutive equations (A2a)–(A2c), this yields

$$\frac{\partial}{\partial r} \left[\frac{1}{r^2} \frac{\partial}{\partial r} (r^2 u) + \alpha \frac{1+\nu}{1-\nu} \theta \right] = 0 \quad (\text{A3})$$

In the dynamic problem at hand, both the displacement and occupancy (sorbed concentration) fields within the coal particle will in general be time dependent. Integration of equation (A3) must therefore yield a solution of the form

$$\frac{1}{r^2} \frac{\partial}{\partial r} [r^2 u(r, t)] + \alpha \frac{1+\nu}{1-\nu} \theta(r, t) = f(t) \quad (\text{A4})$$

where the function $f(t)$ is an integration constant independent of position r but dependent on t . This equation can be further integrated to give

$$u(r) = \frac{1}{r^2} \int_0^r -\alpha r^2 \frac{1+\nu}{1-\nu} \theta(r, t) dr + \frac{1}{3} r f(t) \quad (\text{A5})$$

The function $f(t)$ is determined by the boundary conditions. At the external boundary of the spherical particle, i.e., at $r=b$, the normal stress equals the gas pressure P , so we have

$$P = [\sigma_{rr}]_{r=b} = \frac{E}{1-2\nu} \left[\frac{1-\nu}{1+\nu} \frac{\partial u}{\partial r} + \frac{2\nu}{1+\nu} \frac{u}{r} + \alpha \theta \right]_{r=b} = E \left[\frac{2}{b^3} \int_0^b ar^2 \frac{1}{1-\nu} \theta(r, t) dr + \frac{1/3}{1-2\nu} f(t) \right] \quad (A6)$$

which in turn yields

$$f(t) = 3(1-2\nu) \frac{P}{E} - 2 \frac{3\alpha}{b^3} \frac{1-2\nu}{1-\nu} \int_0^b r^2 \theta(r, t) dr \quad (A7)$$

Substituting this into equations (A2a)–(A2c) and (A5), we obtain the following relations for the displacement and total stress fields inside the sample:

$$u(r, t) = -\frac{\alpha}{r^2} \frac{1+\nu}{1-\nu} \int_0^r r^2 \theta(r, t) dr - 2 \frac{\alpha r}{b^3} \frac{1-2\nu}{1-\nu} \int_0^b r^2 \theta(r, t) dr + r(1-2\nu) \frac{P}{E} \quad (A8a)$$

$$\sigma_{rr}(r, t) = \frac{-\alpha E}{1-\nu} \left\{ \frac{2}{b^3} \int_0^b r^2 \theta(r, t) dr - \frac{2}{r^3} \int_0^r r^2 \theta(r, t) dr \right\} + P \quad (A8b)$$

$$\sigma_{\phi\phi}(r, t) = \frac{-\alpha E}{1-\nu} \left\{ \frac{1}{r^3} \int_0^r r^2 \theta(r, t) dr + \frac{2}{b^3} \int_0^b r^2 \theta(r, t) dr - \theta(r, t) \right\} + P \quad (A8c)$$

$$\bar{\sigma} = \frac{-2E\alpha}{1-\nu} \left(\frac{1}{b^3} \int_0^b r^2 \theta dr - \frac{1}{3} \theta \right) + P \quad (A8d)$$

$$\tau_{\max} = \frac{1}{2} |\sigma_{rr}(r, t) - \sigma_{\phi\phi}(r, t)| = \frac{\alpha E}{2(1-\nu)} \left[\frac{3}{r^3} \int_0^r r^2 \theta(r, t) dr - \theta(r, t) \right] \quad (A8e)$$

At the boundary, i.e., at $r=b$, we therefore have

$$u(b, t) = -\frac{3\alpha}{b^2} \int_0^b r^2 \theta(r, t) dr + b(1-2\nu) \frac{P}{E} \quad (A9a)$$

$$\varepsilon_r(b, t) = -\frac{3\alpha}{b^3} \int_0^b r^2 \theta(r, t) dr + (1-2\nu) \frac{P}{E} \quad (A9b)$$

$$\sigma_{rr}(b, t) = P \quad (A9c)$$

$$\sigma_{\phi\phi}(b, t) = \frac{-\alpha E}{1-\nu} \left\{ \frac{3}{b^3} \int_0^b r^2 \theta(r, t) dr - \theta(r, t) \right\} + P \quad (A9d)$$

Acknowledgments

The China Scholarship Council and Total S.A. are gratefully acknowledged for their financial support of first author Jinfeng Liu and of the research project. The data for this paper are available by contacting the corresponding author at j.liu1@uu.nl.

References

- Balluffi, R. W., S. Allen, and W. C. Carter (2005), *Kinetics of Materials*, pp. 47–68, John Wiley, N. J.
- Battistutta, E., P. Van Hemert, M. Lutynski, H. Bruining, and K.-H. Wolf (2010), Swelling and sorption experiments on methane, nitrogen and carbon dioxide on dry Selar Cornish coal, *Int. J. Coal Geol.*, *84*(1), 39–48.
- Busch, A., and Y. Gensterblum (2011), CBM and CO₂-ECBM related sorption processes in coal: A review, *Int. J. Coal Geol.*, *87*(2), 49–71.
- Busch, A., Y. Gensterblum, B. M. Krooss, and R. Litke (2004), Methane and carbon dioxide adsorption–diffusion experiments on coal: Upscaling and modeling, *Int. J. Coal Geol.*, *60*(2), 151–168.
- Clarkson, C., and R. Bustin (1999), The effect of pore structure and gas pressure upon the transport properties of coal: A laboratory and modeling study. 2. Adsorption rate modeling, *Fuel*, *78*(11), 1345–1362.
- Cui, X., R. M. Bustin, and G. Dipple (2004), Selective transport of CO₂, CH₄, and N₂ in coals: Insights from modeling of experimental gas adsorption data, *Fuel*, *83*(3), 293–303.
- Cui, X., R. M. Bustin, and L. Chikatamarla (2007), Adsorption-induced coal swelling and stress: Implications for methane production and acid gas sequestration into coal seams, *J. Geophys. Res.*, *112*, B10202, doi:10.1029/2004JB003482.
- Day, S., R. Fry, R. Sakurovs, and S. Weir (2010), Swelling of coals by supercritical gases and its relationship to sorption, *Energy Fuels*, *24*, 2777–2783.
- Day, S., R. Fry, and R. Sakurovs (2012), Swelling of coal in carbon dioxide, methane and their mixtures, *Int. J. Coal Geol.*, *93*, 40–48.
- Dutta, P., S. Bhowmik, and S. Das (2011), Methane and carbon dioxide sorption on a set of coals from India, *Int. J. Coal Geol.*, *85*(3), 289–299.
- Espinoza, D., M. Vandamme, J.-M. Pereira, P. Dangla, and S. Vidal-Gilbert (2014), Measurement and modeling of adsorptive–poromechanical properties of bituminous coal cores exposed to CO₂: Adsorption, swelling strains, swelling stresses and impact on fracture permeability, *Int. J. Coal Geol.*, *134*, 80–95.
- Fokker, P. A., and L. G. H. van der Meer (2004), The injectivity of coalbed CO₂ injection wells, *Energy*, *29*(9), 1423–1429.

- Fry, R., S. Day, and R. Sakurovs (2009), Moisture-induced swelling of coal, *Int. J. Coal Prep. Util.*, 29(6), 298–316.
- Fujioka, M., S. Yamaguchi, and M. Nako (2010), CO₂-ECBM field tests in the Ishikari Coal Basin of Japan, *Int. J. Coal Geol.*, 82(3), 287–298.
- Gensterblum, Y., A. Merkel, A. Busch, and B. M. Krooss (2013), High-pressure CH₄ and CO₂ sorption isotherms as a function of coal maturity and the influence of moisture, *Int. J. Coal Geol.*, 118, 45–57.
- Gensterblum, Y., A. Busch, and B. M. Krooss (2014), Molecular concept and experimental evidence of competitive adsorption of H₂O, CO₂ and CH₄ on organic material, *Fuel*, 115, 581–588.
- Goodman, A., R. Favors, and J. W. Larsen (2006), Argonne coal structure rearrangement caused by sorption of CO₂, *Energy Fuels*, 20(6), 2537–2543.
- Govindjee, S., and J. C. Simo (1993), Coupled stress-diffusion: Case II, *J. Mech. Phys. Solids*, 41(5), 863–887.
- Gruszkiewicz, M., M. Naney, J. Blencoe, D. R. Cole, J. C. Pashin, and R. E. Carroll (2009), Adsorption kinetics of CO₂, CH₄, and their equimolar mixture on coal from the Black Warrior Basin, West-Central Alabama, *Int. J. Coal Geol.*, 77(1), 23–33.
- Haward, R. N., and R. J. Young (Eds.) (2012), *The Physics of Glassy Polymers*, 2nd ed., pp. 89–128, Springer, London.
- Hetnarski, R. B., M. R. Eslami, and G. Gladwell (2009), *Thermal Stresses: Advanced Theory and Applications*, pp. 254–260, Springer, New York.
- Hol, S., and C. J. Spiers (2012), Competition between adsorption-induced swelling and elastic compression of coal at CO₂ pressures up to 100 MPa, *J. Mech. Phys. Solids*, 60(11), 1862–1882.
- Hol, S., C. J. Peach, and C. J. Spiers (2011), Applied stress reduces the CO₂ sorption capacity of coal, *Int. J. Coal Geol.*, 85(1), 128–142.
- Hol, S., C. J. Spiers, and C. J. Peach (2012a), Microfracturing of coal due to interaction with CO₂ under unconfined conditions, *Fuel*, 97, 569–584.
- Hol, S., C. J. Peach, and C. J. Spiers (2012b), Effect of 3-D stress state on adsorption of CO₂ by coal, *Int. J. Coal Geol.*, 93, 1–15.
- Hui, C. Y., K. C. Wu, R. C. Lasky, and E. J. Kramer (1987a), Case-II diffusion in polymers. II. Steady-state front motion, *J. Appl. Phys.*, 61(11), 5137–5149.
- Hui, C. Y., K. C. Wu, R. C. Lasky, and E. J. Kramer (1987b), Case-II diffusion in polymers. I. Transient swelling, *J. Appl. Phys.*, 61(11), 5129–5136.
- Karacan, C. Ö. (2003), Heterogeneous sorption and swelling in a confined and stressed coal during CO₂ injection, *Energy Fuels*, 17(6), 1595–1608.
- Karacan, C. Ö. (2007), Swelling-induced volumetric strains internal to a stressed coal associated with CO₂ sorption, *Int. J. Coal Geol.*, 72(3), 209–220.
- Larsen, J. W. (2004), The effects of dissolved CO₂ on coal structure and properties, *Int. J. Coal Geol.*, 57(1), 63–70.
- Larsen, J. W., T. K. Green, and J. Kovac (1985), The nature of the macromolecular network structure of bituminous coals, *J. Org. Chem.*, 50(24), 4729–4735.
- Laxminarayana, C., and P. J. Crosdale (1999), Role of coal type and rank on methane sorption characteristics of Bowen Basin, Australia coals, *Int. J. Coal Geol.*, 40(4), 309–325.
- Levine, J. R. (1996), Model study of the influence of matrix shrinkage on absolute permeability of coal bed reservoirs, *Geol. Soc. London, Spec. Publ.*, 109(1), 197–212.
- Liu, J., Z. Chen, D. Elsworth, H. Qu, and D. Chen (2011), Interactions of multiple processes during CBM extraction: A critical review, *Int. J. Coal Geol.*, 87(3), 175–189.
- Liu, J., C. J. Peach, and C. J. Spiers (2016a), Anisotropic swelling behaviour of coal matrix cubes exposed to water vapour: Effects of relative humidity and sample size, *Int. J. Coal Geol.*, 167, 119–135.
- Liu, J., C. J. Spiers, C. J. Peach, and S. Vidal-Gilbert (2016b), Effect of lithostatic stress on methane sorption by coal: Theory vs. experiment and implications for predicting in-situ coalbed methane content, *Int. J. Coal Geol.*, 167, 48–64.
- Mazumder, S., and K. H. Wolf (2008), Differential swelling and permeability change of coal in response to CO₂ injection for ECBM, *Int. J. Coal Geol.*, 74(2), 123–138.
- Mazumder, S., F. Vermolen, and J. Bruining (2011), Analysis of a model for anomalous-diffusion behavior of CO₂ in the macromolecular-network structure of coal, *SPE J.*, 16(04), 856–863.
- Merkel, A., Y. Gensterblum, B. M. Krooss, and A. Amann (2015), Competitive sorption of CH₄, CO₂ and H₂O on natural coals of different rank, *Int. J. Coal Geol.*, 150, 181–192.
- Myers, A. (2002), Thermodynamics of adsorption in porous materials, *Aiche J.*, 48(1), 145–160.
- Pan, Z., and L. D. Connell (2007), A theoretical model for gas adsorption-induced coal swelling, *Int. J. Coal Geol.*, 69(4), 243–252.
- Peng, Y., J. Liu, M. Wei, Z. Pan, and L. D. Connell (2014), Why coal permeability changes under free swellings: New insights, *Int. J. Coal Geol.*, 133, 35–46.
- Pini, R., S. Ottiger, L. Burlini, G. Storti, and M. Mazzotti (2010), Sorption of carbon dioxide, methane and nitrogen in dry coals at high pressure and moderate temperature, *Int. J. Greenhouse Gas Control*, 4(1), 90–101.
- Pini, R., G. Storti, and M. Mazzotti (2011), A model for enhanced coal bed methane recovery aimed at carbon dioxide storage, *Adsorption*, 17(5), 889–900.
- Pone, J. D. N., P. M. Halleck, and J. P. Mathews (2009), Sorption capacity and sorption kinetic measurements of CO₂ and CH₄ in confined and unconfined bituminous coal, *Energy Fuels*, 23(9), 4688–4695.
- Setzmann, U., and W. Wagner (1991), A new equation of state and tables of thermodynamic properties for methane covering the range from the melting line to 625 K at pressures up to 100 MPa, *J. Phys. Chem. Ref. Data*, 20(6), 1061–1155.
- Shewmon, P. (1989), *Diffusion in Solids*, 2nd ed., pp. 30–32, The Minerals, Metals and Materials Society, Warrendale, Pa.
- Shi, J.-Q., and S. Durucan (2003), A bidisperse pore diffusion model for methane displacement desorption in coal by CO₂ injection, *Fuel*, 82(10), 1219–1229.
- Staib, G., R. Sakurovs, and E. M. A. Gray (2013), A pressure and concentration dependence of CO₂ diffusion in two Australian bituminous coals, *Int. J. Coal Geol.*, 116, 106–116.
- Staib, G., R. Sakurovs, and E. M. A. Gray (2014), Kinetics of coal swelling in gases: Influence of gas pressure, gas type and coal type, *Int. J. Coal Geol.*, 132, 117–122.
- Suuberg, E. M., Y. Otake, Y. Yun, and S. C. Deevi (1993), Role of moisture in coal structure and the effects of drying upon the accessibility of coal structure, *Energy Fuels*, 7(3), 384–392.
- Thomas, N. L., and A. Windle (1982), A theory of case II diffusion, *Polymer*, 23(4), 529–542.
- van Bergen, F., H. Pagnier, and P. Krzystolik (2006), Field experiment of enhanced coalbed methane-CO₂ in the upper Silesian basin of Poland, *Environ. Geosci.*, 13(3), 201–224.
- van Bergen, F., C. Spiers, G. Floor, and P. Bots (2009), Strain development in unconfined coals exposed to CO₂, CH₄ and Ar: Effect of moisture, *Int. J. Coal Geol.*, 77(1–2), 43–53.
- Zhao, Y., S. Liu, Y. Jiang, K. Wang, and Y. Huang (2016), Dynamic tensile strength of coal under dry and saturated conditions, *Rock Mech. Rock Eng.*, 49, 1709–1720.